ISTANBUL TECHNICAL UNIVERSITY ★ GRADUATE SCHOOL

CLOSED-LOOP FLOW SEPARATION CONTROL IN THE BACKWARD FACING STEP FLOW USING FUZZY-BASED PID CONTROLLER

M.Sc. THESIS

Hamed RAHMATI AYDENLOU

Department of Mechanical Engineering

Heat Fluid Programme

SEPTEMBER 2022

ISTANBUL TECHNICAL UNIVERSITY ★ GRADUATE SCHOOL

CLOSED-LOOP FLOW SEPARATION CONTROL IN THE BACKWARD FACING STEP FLOW USING FUZZY-BASED PID CONTROLLER

M.Sc. THESIS

Hamed RAHMATI AYDENLOU
(5031881111)

Department of Mechanical Engineering

Heat Fluid Programme

Thesis Advisor: Asst. Prof. Dr. Abdussamet SUBAŞI

SEPTEMBER 2022

İSTANBUL TEKNİK ÜNİVERSİTESİ ★ LİSANSÜSTÜ EĞİTİM ENSTİTÜSÜ

BULANIK TABANLI PID KONTROLCÜ KULLANARAK GERİ BASAMAK AKIŞININ KAPALI DÖNGÜ AKIŞ AYIRMA KONTROLÜ

YüKSEK LİSANS TEZİ

Hamed RAHMATI AYDENLOU
(5031881111)

Makina Mühendisliği Anabilim Dalı

Isı Akışkan Programı

Tez Danışmanı: Dr. Öğr. Üyesi Abdussamet SUBAŞI

EYLÜL 2022

Hamed RAHMATI AYDENLOU, a M.Sc. student of ITU Graduate School student ID 5031881111, successfully defended the thesis entitled "CLOSED-LOOP FLOW SEPARATION CONTROL IN THE BACKWARD FACING STEP FLOW USING FUZZY-BASED PID CONTROLLER", which he/she prepared after fulfilling the requirements specified in the associated legislations, before the jury whose signatures are below.

Thesis Advisor :	**Asst. Prof. Dr. Abdussamet SUBAŞI** Istanbul Technical University	.....
Jury Members :	**Prof. Dr. Bayram ŞAHİN** Istanbul Technical University	.....
	Assoc. Prof. Dr. Mehmed Rafet ÖZDEMİR Marmara University	.....

Date of Submission : 26 September 2022
Date of Defense : 29 September 2022

To my family,

FOREWORD

It is an honor for me to heartily thank my advisor, Asst. Prof. Dr. Abdussamet SUBAŞI, whose encouragement, patience and generous support from the beginning to the very last days enabled me to develop an understanding of the subject. Dr. Subaşı who has the attitude and substance of an effective supervisor has continually conveyed a spirit of research in regard to this topic. I must honestly say that without his help this thesis would not have been completed. Additionally, I offer my best regards and blessings to my family, my father, mother and my brother whose supports have been always with me during this path and all of my friends especially Shervin Ataeian who supported me in any respect towards the completion of my thesis.

September 2022

Hamed RAHMATI AYDENLOU
(Mechanical Engineer)

TABLE OF CONTENTS

Page

ABBREVIATIONS

BFS : Backward Facing Step [-]
BW : Back Wall boundary condition [-]
CFD : Computational Fluid Dynamics [-]
D_{MF} : Degree of Membership Function [-]
FEM : Finite Element Method
FEW : Front Extension Wall boundary condition [-]
FMW : Front main Inlet boundary condition [-]
FVM : Finite Volume Method
f : frequency [Hz]
GAO : Genetic Algorithm Optimization [-]
h_i : Height of main inlet flow [m]
h_s : Height of the step wall [m]
NFE : Number of Function Evaluation
NC : Number of Cells [-]
OS : Overshoot [s]
PSO : Particle Swarm Optimization [-]
RL : Recirculation Length [-]
RS : Random Selection [-]
RWS : Roulette Wheel Selection[-]
SW : Step Wall boundary condition [-]
TS : Tournament Selection [-]
u(y) : profile of the main inlet velocity [ms^{-1}]
VI : Velocity inlet boundary condition [-]
ZNMF : Zero Net Mass Flux [-]
Z-N : Ziegler-Nichols [-]

SYMBOLS

A	: Cross section area [m^2]
AR	: Aspect Ratio [-]
C_D	: Drag coefficient[-]
$C_{f,x}$	: Friction drag coefficient (Skin Friction Coefficient) [-]
CF	: Cost Function [s]
CF_{norm}	: Normalized cost function [-]
$CF^{norm}_{OptFPID}$	: Normalized cost function of the optimized fuzzy-PID controller[-]
CF^{norm}_{FPID}	: Normalized cost function of the fuzzy-PID controller[-]
CFL	: Courant number [-]
ER	: Expansion Ratio [-]
F_D	: Drag force [N]
F_i^{norm}	: Normalized value of the individual in the cost function
F_i^{min}	: Minimum value of the individual in the cost function
K_{d}	: Derivative gain
K_{d}'	: Normalized Derivative gain
K_i	: Integral gain
K_{p}	: Proportional gain
K_{p}'	: Normalized Proportional gain
K_u	: Ultimate gain
T_d	: Derivative time [s]
T_i	: Integration time [s]
T_u	: Oscillation period [s]
$\dot{Q}_{\mathbf{o}}(t)$	: Mass flow rate through the orifice
RT	: Rising Time[s]
RT_{norm}	: Normalized rising Time[-]
ST	: Settling Time [s]
ST_{norm}	: Normalized settling Time[-]
U_{peak}	: Maximum value of the jet velocity [ms^{-1}]
U_∞	: Maximum value of the main inlet velocity [ms^{-1}]
α	: Normalized parameter implying Integral gain [-]
V_{SJ}	: Velocity of Synthetic Jet [ms^{-1}]
Δ	: Diaphragm oscillation amplitude [m]
υ	: Kinematic viscosity [m^2s]
ρ	: Fluid density [kgm^{-3}]
μ	: Dynamic viscosity [$kgm^{-1}s^{-1}$]
τ_w	: X-wall shear stress [Nm^{-2}]

LIST OF TABLES

Page

LIST OF FIGURES

Page

CLOSED-LOOP FLOW SEPARATION CONTROL IN THE BACKWARD FACING STEP FLOW USING FUZZY-BASED PID CONTROLLER

SUMMARY

Fluid flow around solid bodies from rudimentary to sophisticated, is one of the spotlights in fluid dynamic analysis which includes various phenomena such as flow separation. Flow separation is an important engineering topic which has been considered in various internal and external flow problems leading to pressure drag, loss of lift, stall, pressure recovery losses and vortex shedding leading to significant failure in the resonance frequency domain. The problem which has become benchmark regarding the flow separation and reattachment length is the Backward Facing Step. Despite of having tremendous theoretical, numerical, and experimental studies related to this problem, there have been less value of research regarding the flow control in this geometry. Having reattachment after separation of the flow in this geometry increases the unsteadiness, pressure fluctuations, vibrations and noise disturbances. Among the various actuators employed for ameliorating aforementioned issue, the synthetic jet known actuator has been notified. In the beginning of this study, the sinusoidal synthetic configuration has been investigated, and related equations have been extracted. In order of comparing the results, two cases of studies including without and with jet were studied. In the first part of study, the numerical analysis has been conducted to validate the gathered results from the reference studies in the literature using ANSYS FLUENT. The results have concluded that simulation results had the acceptable agreement with the previously conducted reference studies. In the next step, the main Computational Fluid Dynamics simulation part of this study including the single sinusoidal synthetic jet over the step wall was carried out in three different Reynolds numbers as 200, 300, and 400. Having carried out the simulation related to the with-jet case, discrete transfer function was extracted using systemIdentification toolbox of MATLAB. The transfer function with 5 poles and 4 zeros reached the desirable agreement with the reference data. The achieved transfer function was utilized in the SIMULINK models being designed for testing the various Proportional-Integral-Differential (PID) controller configurations. Three types of conventional, Fuzzy and optimized fuzzy PID controllers were considered for investigation and comparison. Three gains including proportional (K_p'), integral (α) and derivative (K_d') of the PID controller were tuned based on classical Ziegler–Nichols and Fuzzy Inference System (FIS). The results revealed that the fuzzy-PID controller has better efficiency regarding the overshoot, rising time and settling time criteria in comparison with conventional PID controller. To reach the better performance of the fuzzy-PID controller, two methods of genetic algorithm and particle swarm optimization methods were employed. Subsequently, the optimized

fuzzy inference system from this method was inserted in the SIMULINK model and optimized fuzzy PID controller was constructed. The comparison between three defined PID controllers (conventional, fuzzy, optimized fuzzy) were conducted using the designed SIMULINK model. The results showed that the least values of overshoot, rising time and settling was belonging to the optimized fuzzy PID controller based on defined cost function criteria. After that, instead of applying the extracted transfer function, ANSYS FLUENT was coupled with SIMULINK. The obtained results revealed that the designed PID controller was able to define a desirable amplitude for the jet where the fluctuation of the drag coefficient has been eliminated and the magnitude of the recirculation length became less than value of the without jet case of study by 17.35 %. Furthermore, eliminating the fluctuations of the drag coefficient leads to less consuming energy of the jet which is the another benefits of the applying optimized fuzzy-PID controller. Finally, the results are investigated in detail considering the undelying physical phenomena around the step wall. In the next step, the main CFD simulation part of this study including the single sinusoidal synthetic jet over the step wall was carried out in three different Reynolds numbers as 200, 300, and 400. Having carried out the simulation related to the with-jet case, discrete transfer function related to the 400 Reynolds number was extracted using systemIdentification toolbox of MATLAB. The transfer function with 5 poles and 4 zeros reached the desirable agreement with the reference data, and validated based on 200 and 300 Reynolds numbers. The achieved transfer function was utilized in the SIMULINK models being designed for testing the various upcoming Proportional-Integral-Differential (PID) controller configurations. Three types of conventional, Fuzzy and optimized fuzzy PID controllers were considered for investigation and comparison. Three gains including proportional ($K_p{}'$), integral (α) and derivative ($K_d{}'$) of the PID controller were tuned based on classical Ziegler–Nichols and Fuzzy Inference System (FIS). The results revealed that the fuzzy-PID controller has better efficiency regarding the overshoot, rising time and settling time criteria in comparison with conventional PID controller. To reach the better performance of the fuzzy-PID controller, two methods of genetic algorithm and particle swarm optimization methods were employed. The tournament selection method based on bisector defuzzification showed the least value of the cost function and Number of Function Evaluation with respect two other selection methods. Subsequently, the optimized fuzzy inference system from this method was inserted in the SIMULINK model and optimized fuzzy PID controller was constructed. The comparison between three defined PID controllers (conventional, fuzzy, optimized fuzzy) were conducted using the designed SIMULINK model. The results showed that the least values of overshoot, rising time and settling was belonging to the optimized fuzzy PID controller based on normalized cost function criteria. After that, instead of applying the extracted transfer function, ANSYS FLUENT was coupled with SIMULINK. The obtained results revealed that the designed PID controller was able to define a desirable amplitude for the jet where the fluctuation of the drag coefficient has been eliminated and the magnitude of the recirculation length became less than value of the without jet case of study by 17.35 %. Additionally, the results depicted that the designed SIMULINK model with considering the optimized fuzzy-PID controller is able to reach the defined drag coefficient being less than the sinusoidal jet without PID case of study. Furthermore, eliminating the fluctuations of the drag coefficient leads to less consuming energy of the jet which is the another benefits of the applying

optimized fuzzy-PID controller. Finally, the dimensional analysis of the fluid physical phenomena around the step wall was conducted. The results concluded that the height and width of the secondary vortex for the with sinusoidal jet tuned by optimized fuzzy PID controller is higher than the without-jet case of study.

BULANIK TABANLI PID KONTROLCÜ KULLANARAK GERİ BASAMAK AKIŞININ KAPALI DÖNGÜ AKIŞ AYIRMA KONTROLÜ

ÖZET

Akış ayrılması gibi çeşitli olguları içeren katı cisimlerin etrafındaki akışkan akışı, akışkan dinamiği analizindeki ilgi çekici konulardan biridir. Akış ayırması; basınç direnci, kaldırma kaybı, durma ve basınç geri kazanım kayıpları gibi çeşitli fiziksel olaylarla doğrudan ilgili olduğundan iç ve dış akış problemlerinde ele alınan önemli araştırma konularından biridir. Akış ayrılması ve akışın yeniden tutunma mesafesi problemlerinde geri basamak akışı üzerinde temel çalışmaların yapıldığı bir referans haline gelmiştir. Literatürde geri basamak akışını konu edinen çok sayıda teorik, sayısal ve deneysel çalışma olmasına rağmen çeşitli akış kontrol yöntemlerinin geri basamak akışına uygulanması ile ilgili araştırmaların sayısı görece daha azdır. Geri basamak akışında meydana gelen akış ayrılmasından sonra yeniden bağlanma olması; kararsızlığı, basınç dalgalanmalarını, titreşimleri ve gürültü bozukluklarını artırdığı, bu olumsuzlukların giderilmesi ya da etkisinin azaltılması için sentetik jet kullanımının literatürde yaygın olduğu bilinmektedir. Bu çalışma kapsamında öncelikle, sinüzoidal sentetik jet konfigürasyonunun etkisi sayısal olarak araştırılmıştır. Sinüzoidal jetin etkisini belirleyebilmek için jetsiz ve jetli olmak üzere iki ayrı vaka çalışması yapılmıştır. Nihai simülasyonlardan önce çözüm ağından ve zaman adımından bağımsızlık çalışması ve literatürden seçilen referans çalışmalar üzerinden jetli ve jetsiz durum için doğrulama çalışması yapılmıştır. Elde edilen sonuçların literatür ile kabul edilebilir seviyede uyumlu olduğu tespit edildikten sonra nihai analizler gerçekleştirilmiştir. Bu kapsamda, basamak duvarına yerleştirilen jetin etkisi 200, 300 ve 400 olmak üzere üç farklı Reynolds sayısında incelenmiştir. Kontrolcü parametrelerinin tespit edilmesinde kullanılmak üzere MATLAB'in systemIdentification araç kutusu kullanılarak transfer fonksiyonu elde edilmiştir. Elde edilen 5 kutuplu ve 4 sıfırlı transfer fonksiyonunun tüm Reynolds sayıaları için ele alınan sistemi kabul edilebilir seviyede tespit edildiği tespit edilmiştir. Elde edilen transfer fonksiyonu, Oransal-İntegral-Diferansiyel (PID) kontrolcünün parametrelerini ayarlamak için oluşturulan SIMULINK modellerinde kullanılmıştır. PID kontrolcünün parametreleri (K_p', α ve K_d'); Ziegler–Nichols ve Bulanık Çıkarım Sistemi (bulanık-PID) olmak üzere iki farklı yöntem kullanılarak belirlenmiştir. Bulanık-PID kontrolcünün geleneksel yöntemler kullanılan PID kontrolcüye kıyasla aşma, yükselme ve yerleşme süresi kriterleri dikkate alındığında daha iyi sonuç verdiği tespit edilmiştir. Bulanık-PID denetleyicinin performansını arttırmak için genetik algoritma ve parçacık sürüsü olmak üzere iki farklı optimizasyon yöntemi kullanılmıştır. SIMULINK modeli üzerinden parametreleri üç farklı yöntem (geleneksel, bulanık, optimize edilmiş bulanık) kullanılarak ayarlanmış olan PID

kontrolcülerin performansı kıyaslanmıştır. Aşma, yükselme ve yerleşme süresi dikkate alındığında optimize edilmiş bulanık PID kontrolörün diğerlerine kıyasla daha iyi sonuç verdiği tespit edilmiştir. Daha sonra SIMULINK modelinde yer alan sistemin transfer fonksiyonu yerine MATLAB ile ANSYS FLUENT'in birbiriyle konuşması sağlanarak ANSYS FLUENT simülasyonu yerleştirilmiş ve ANSYS FLUENT simülasyonlarındaki sentetik jetin hızının tasarlanan PID kontrolcü ile gerçek zamanlı kontrol edildiği simülasyonlar yapılmıştır. Elde edilen sonuçlar dikkate alınarak, tasarlanan PID kontrolörünün, sürükleme katsayısındaki dalgalanmayı ortadan kaldırıldığı ve ayrılmış akış bölgesi uzunluğunun, jetsiz çalışma durumuna kıyasla % 17.35'e kadar düşürdüğü tespit edilmiştir. Ayrıca, sürükleme katsayısındaki dalgalanmaların ortadan kaldırılması, optimize edilmiş bulanık-PID kontrolörünün uygulanmasının sentetik jetin daha az enerji tüketmesine yol açtığı belirlenmiştir. Son olarak, basamak duvarının etrafındaki akış yapısı altta yatan fiziksel olaylar da dikkate alınarak ayrıntılı olarak araştırılmıştır.

1. INTRODUCTION

Fluid flow around solid bodies is one of the most important spotlights in fluid dynamic analysis leading to various phenomena including flow separation and drag enhancement. These solid bodies can be seen in numerous applications from daily life including buildings, trees and automobiles for instance to the most sophisticated devices including aircrafts. Flow separation is the phenomenon which can lead to the noise disturbances, pressure fluctuations and drag increment, consequently, leading to fuel consumption and device failure. Beside of reducing the noise disturbances, the bonus effect of dispersing the flow separation will be the reduction of the drag coefficient which result in less fuel consumption and emission released to the atmosphere. The impact of reducing the drag can be deeply sensed where reducing 1% of it returns with the 0.75% reducing the fossil fuels of a jet airliner under cruise conditions, meaning, decreasing 9 million tons of CO_2 emission. Due to this reason, having profound understanding related to the flow separation is the obligation of the engineering community to design a more efficient systems by having comprehensive knowledge of the subject [1].

1.1 Flow Separation

Flow separation phenomenon and subsequent reattachment because of the sudden expansion and compression in turbulent and laminar flow domains is a trending engineering problem which could be prescribed as the most important and challenging topic of the fluid dynamics. The flow separation leads to the loss of energy, deviation of stream lines and reverse flow which causes enhancement of the drag coefficient in external flows while stall reduces efficiency for the internal flows. Studies around 1960 showed that the boundary layer theory at that moment was not able to predict the separation and still, after four decades of research related to this topic, several aspects of fluid motions behavior are still not fully understood, especially from the standpoint of time dependency [2]. Flow separation in external and internal flows have

different types of behaviors caused by confinement of the walls and specific considered design [3]. The separation and reattachment can be seen in various internal systems including turbines, diffuser and combustors in addition to external systems such as aircrafts and buildings [4]. The reason that the flow separation occurs is having the inflection point in the velocity profile while the velocity at the wall is zero or negative. Having adverse pressure gradient in the cross-flow or having geometric discontinuity including sharp turns, higher angles of attack as well as other reasons are leading to flow separation. Thickening the secondary flow region adjacent to the surface and increasing the value of the velocity in the wall-normal directions are the outcomes of the flow separation resulting in enhancement of the pressure drag, loss of lift, stall, pressure recovery losses and vortex shedding which can lead to significant failures in the resonance frequency domain [5]. The majority of the studies related to the flow separation has been conducted based on Backward Facing Step (BFS) geometry as the benchmark problem in experimental, theoretical and computational investigations so far with various flow configurations and modifications due to following reasons. First, this problem demonstrates the essential features of the separated flows in addition to the capability in simplifications which shows the deep interest in understanding instability and transition to turbulence in non-parallel open flows. Secondly, due to having extensive data of conducted studies, the comparison would be more possible. Third, flow resulted from abrupt changes in the geometry is of a great importance in many engineering applications including various fields from aerodynamic devices such as high-lift airfoils at large angles of attack to complex architecture of buildings as depicted in Figure 1.1 [3]. In the flow separation problem of the BFS, free shear layer evolution is the key element. Therefore, the most important factors of investigating this geometry are the free shear separation, vortex evolution and reattachment length as shown in Figure 1.2 [3]. The reattachment point in the BFS is the point where the skin coefficient changes from negative to positive. Geometry of the BFS includes dimensionless parameters which have been investigated regarding their effectiveness in reducing the flow separation issue. The Expansion Ratio (ER) and Aspect Ratio (AR) are the most important ones which have been reported frequently in previous articles. The ER of the duct can be obtained using equation (1.1) [4].

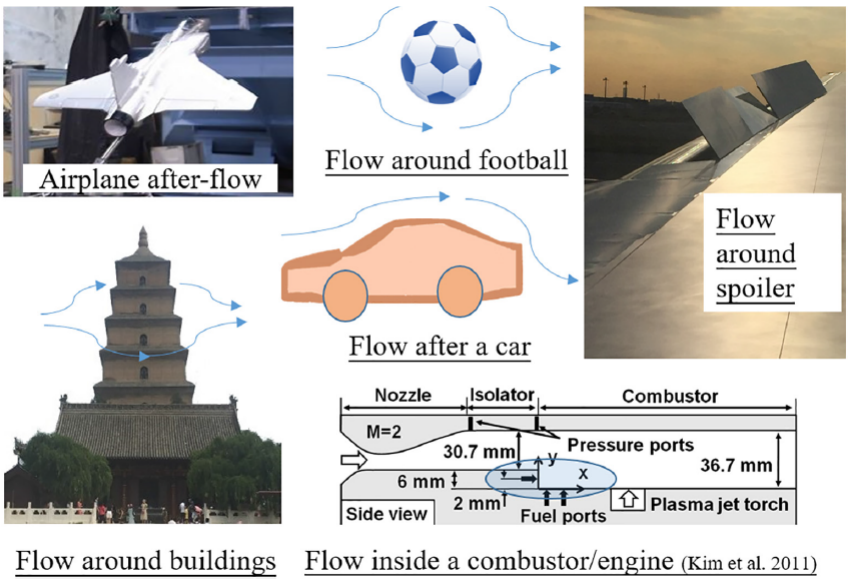

Figure 1.1 : Various applications the BFS geometry has been applied [3].

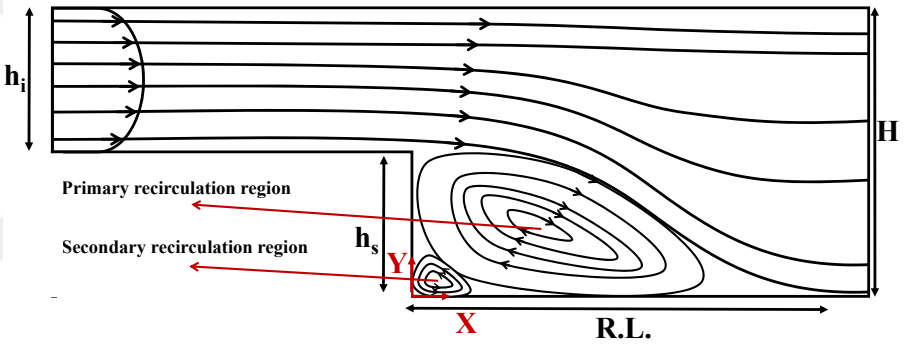

Figure 1.2 : Flow behaviour around the BFS geometry, inspired by [6].

$$ER = \frac{H}{H - h_s} \tag{1.1}$$

Similarly, AR can be calculated based on the ratio of the width to height of the step, as demonstrated in equation (1.2) [4].

$$AR = \frac{W}{h_s} \tag{1.2}$$

In this geometry, both shear-layer and shedding-type instability are involved in the promotion of the reattachment length. These two are the sources for the roll-up process of shear layer and shear layer interaction with the wall respectively. The shear layer has a significant effect on forcing since if the disturbance can be intensified by the shear layer, interaction with the wall occurs faster and consequently reattachment

length will be smaller due to having large vertical structures [7]. The presence of the separated flow and subsequently, the reattaching flow enhance the unsteadiness as well as pressure fluctuations, vibrations and noise disturbances. An effective and successful flow control, which helps to reduce the recirculation length can be only achieved by a profound understanding of underlying physics of the flow separation and reattachment phenomena. Therefore, the focus of this research will be over the flow control method which reduces the flow separation and consequently, drag coefficient in a meaningful way.

1.2 Flow Control

By applying flow control over the considered system, the efficiency could be increased and the cost of operations could be reduced [8]. Flow control techniques, which have been developing since Prandtl conducted his research over the boundary layer area, can be defined as the collection of techniques that reduce deleterious effects in the fluid flow systems [9, 10]. Within the field of fluid dynamics, in a circumstance where the considered system does not perform in the desired condition, flow control is applied in order of increasing or reducing the undesired value of the parameters with minimum of influence on the system. There has been early interest in developing flow control methods, specifically applying external forces for turbulent and laminar flows in steady or unsteady situations. Drag, lift and pressure fluctuations are the most common parameters which are usually targeted for controlling. Specifically, the flow control can be summarized mostly in four applications including drag reduction, lift augmentation, mixing augmentation and noise reduction. Controlling the skin friction, separation on aircraft wings, enhancing mixing ratio in jet engine exhaust are the applicable examples which can be mentioned [4, 7, 9]. Regarding the perspective, classification schemes of flow control could be categorized in two schemes. The first classification scheme is based on applying the method over the wall or not while the other classification scheme is based on whether technique requires energy input or not. Flow control has been dived in two categories as an active and passive techniques according to the latter classification scheme considering the power expenditure of the techniques. Passive flow control is based on no needing for power or control loop. This includes applying techniques such as fixed mechanical vortex generator,

designing specific geometries and adjusting ribs on the surface for separation control, manipulation of pressure gradient and drag reduction [8]. Despite of having simple and low cost devices and not requiring extra input power for the passive flow control methods, two disadvantages of this methods are as following. First that they are unable of optimizing the multiple conditions and secondly they weaken the separation at the defined state while causing massive separation and unnecessary extra drag at the non-defined states [1]. In most of study cases, the limitation for the passive flow control can be sensed due to issues including aesthetics, size, comfort, safety, reliability and cost which are obstacles for the perfect aerodynamic form. However, aforementioned problems is not issues in active flow control methods. Even though, power is an obligation. Active flow control can be organized in two groups including closed and open loop control methods. The difference between the open and closed loop flow control is based on the reaction for changing the operating conditions. In the open loop flow control, action is not based on the observation of the flow while in the closed loop flow control, data from the flow observation is gathered using the installed sensors and the data is utilized to determine the best possible control action. Therefore, it can be stated that the propose of the closed loop flow control methods is the adapting of actuators to the variations in the experimental conditions (external perturbations). Regarding actuators, they have been in the center of attentions among the active flow control devices [8]. There have been various actuators applied in active flow control such as fluidic, thermal, acoustic, piezoelectric, electrodynamic, electromagnetic and shape-memory alloy. List of actuators can be found in the review study done by Fiedler and Fernholz 1990 [11]. One way to classify the actuators are demonstrated in Figure 1.3 where actuators are classified based on their applications. The most common type of actuators is fluidic using fluid injection or suction [10]. Among these actuators, one of which that has been applied in problems related to the boundary layer separation is the synthetic jet known as the zero-net mass-flux (ZNMF) actuator by injecting pulses of high-momentum fluid into boundary layer to delay separation [12].

Synthetic jet operates based on periodic excitation force consisting of an orifice connected to a cavity and oscillates with a weak amplitude to produce flow from the orifice [13]. Even though that the synthetic jets are similar to the pulsed jets, they have a unique feature which is that they are totally created from the working fluid of

the system and therefore can transfer the linear momentum to the flow of the system without net mass injection across the flow boundary [14].

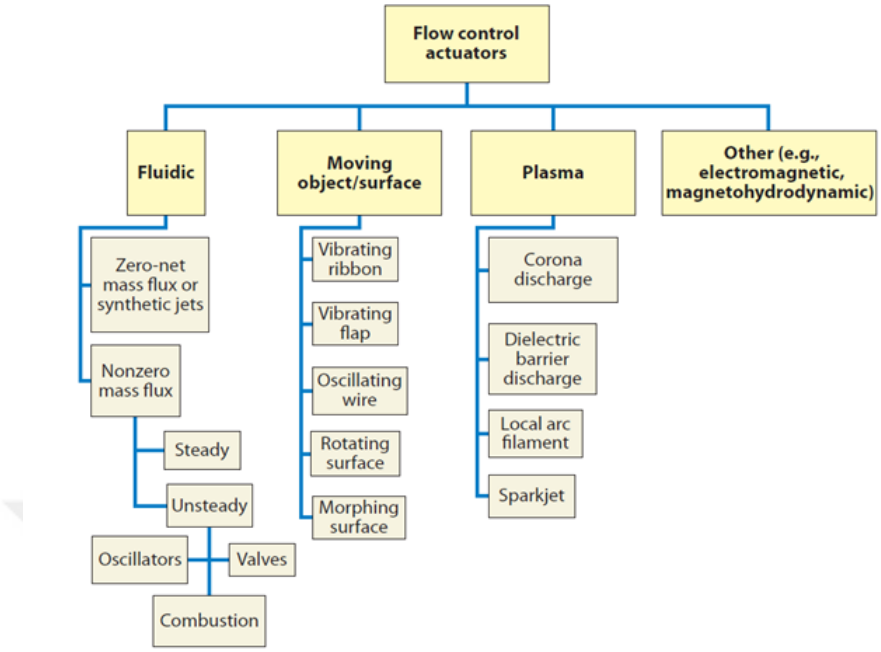

Figure 1.3 : Classifications of the flow control actuators [10].

The main applications of this device is thrust vectoring of jets, enhancement of mixing in shear layer, reducing the separated flow regions and drag in boundary layers [9]. This synthetic jet creates the unsteady forcing which is more effective than the steady forcing. Due to transferring linear momentum without net mass injection, the need for blowing and suction and consequently extra energy requirement is eliminated [5]. Having the active flow control capability beside of their weight and compactness are the advantages of these devices which make them suitable for diverse applications including aircrafts, unmanned and microscale air vehicles and rotorcrafts [13]. Synthetic jets could have various applications. For instance, by controlling the aerodynamic shape of an aircraft using the synthetic jet, fighter can maneuver without defecting a control surface and remains its minimum radar cross section [15]. Synthetic jet operates based on suction or blowing forces. In the blowing period, the jet applies energy into the flow, the new boundary layer overcomes the adverse pressure leading to delay the separation phenomenon beside of enhancing the mixing. In the suction period of the synthetic jet, the transition point will be shifted to the boundary layer which causes decreasing the drag coefficient.

Having these forces at the same device could be privilege. Therefore, the oscillatory blowing and suction will be more effective than simple steady blowing or suction [5]. However, manual adaption of synthetic in the system is tedious nor possible due to instant variation of the working fluid. To fulfill the automatic control of the actuators, various types of controllers have been introduced. Among these, PID controllers are one of the most important components of the closed loop control methods in order of reaching the desirable value of variable in the defined system. Proportional-Integral-derivative (PID) controllers are known as the best controllers in industrial control processes due having simplicity in structure and robust performance in a wide range of operating conditions. PID controllers can be divided in two main categories. In the first one, the parameters of the controller after being tuned or chosen will be fixed during the process. Among these methods, Ziegler-Nichols (Z-N) tuning formula is the most well-known method [16]. Even though PID controllers of this category are simple, due to operating in systems with changing parameters, they cannot work properly. Oppositely, the PID controllers of the second category called adaptive PID controllers, due to updating parameters on-line based on parameter estimation of the system, they operate more efficiently. The growth of the knowledge-based systems in process control can be sensed specially in the field of the fuzzy control, where the linguistic description of human expertise is applied in controlling process based on fuzzy rules and relations. Even though fuzzy logic controllers do not clearly understand the structure of the PID controllers, they may be considered as nonlinear PID controllers whose parameters are determined on-line based on error signal and derivative of the error signal [17]. By applying the fuzzy logic based on judgment of the experienced operator over the PID controller, enhancement of the energy efficiency can be exploited. Fuzzy logic has been an effective method for scheduling the gain coefficients of the conventional PID controllers (Fuzzy-PIDs). Therefore, fuzzy-PID controllers due to having superior robustness and applicability of the fuzzy logic, has been considered as an alternative [18]. Having more efficient fuzzy inference system will lead to have minimum required input energy. This aim can be reached by applying optimizations methods such as Genetic Algorithm Optimization (GAO) [19]. Other methods of optimization have been examined as well. Particle Swarm Optimization (PSO) method, designed by Kennedy and Eberhart et al. 1995 is a swarm intelligence

technique based on stochastic and population-based adaptive method. It has been inspired from the behavior of bird folks and fish swarms. Having had only few parameters to adjust, it provides higher performance and therefore less computation time, higher accuracy and less memory size related to previous proposed methods including machine learning neural computing and genetic computation [20].

1.3 Literature Review

Comprehensive studies have been conducted on the recirculation length and various methods for reducing the unfavorable separation area behind the step [3]. For example, the utilization of the oscillating sharp separation edge and sound waves by influencing the reattachment process have been experimented [21, 22]. It should be pointed out that studies on optimizing the dimensionless parameters including aspect ratio, ER and angle of steps have been carried out both experimentally and numerically. Louda et al. (2013) studied the BFS with different angle of steps including 10, 25, 45 and 90 degrees in both 2D and 3D simulation environments based on Finite Volume Method (FVM) and Finite Element Method (FEM). According to the results, FVM obtained more acceptable results than FEM and had better applicability for 3D simulations of the perpendicular step with negligible deficiency in predicting the reattachment length [23]. Effect of ER was investigated in a study where three values of 0.5, 1 and 2.13 were applied as shown in Figure 1.4 [24]. It has been concluded that the ER strongly affects the development of the turbulence and separated shear layer. Specifically, by increasing the relative value of the step height to inlet channel, the turbulence intensities enhanced which caused the shorter normalized reattachment lengths.

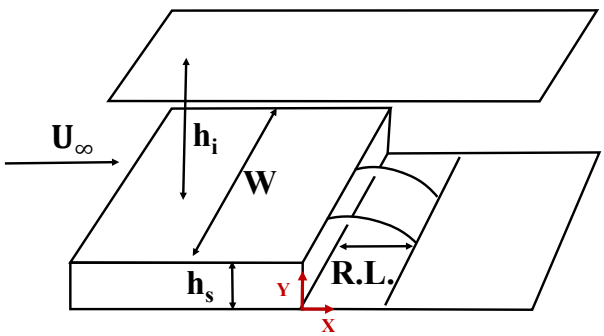

Figure 1.4 : Schematic of the BFS and the main geometrical parameters, inspired by [25].

3D modeling for investigating the effect of the aspect ratio over the recirculation length in the laminar flow domain for Reynolds number around 250 has been conducted by Iwai et al, 2000. The results revealed that the aspect ratio of 16 has the best compatibility with the results achieved from 2D simulation analysis [4]. Armaly et al. (1983) conducted a numerical and experimental over the BFS from laminar to turbulent flow to investigate the velocity distribution and reattachment length. In this study, the aspect ratio was 16 to ensure the accuracy and reliability of the results in two dimension analysis [26]. The results depicted that there is slight difference between the numerical and experimental data where the flow was considered two-dimensional. It is concluded that the distribution of the reattachment length was uniform in spanwise direction except near the side walls where the reattachment length decreased. The novelty of work done by Coskun et al. (2021) was to investigate the effect of using three jets instead of one with constant velocity at three different locations to reduce the recirculation length over the step while increasing the Nusselt number [27]. In this study, 19 different configurations of jet velocity were simulated where the velocity of each jet was the ratio between -2 to 2 with respect to the mean free stream inlet velocity. It should be pointed out that these configurations were defined based on having net zero mass flux in the main domain of investigations. The results indicated that recirculation zone reduced at the positive jet velocity of the jet on the step wall. This also leads to higher value of Nusselt number since recirculation region acted as an insulation area. Uruba et al. (2007) conducted an experiment over the BFS to reduce the length of the reattachment length based on applying only two circumstances of positive and negative domain of velocities (blowing/suction respectively) for the adjusted jet that considered near the step. The results indicated that the suction control mechanism had more effectiveness in reducing the size of the reattachment length than blowing one. Additionally, it has been concluded that the continuous suction/blowing, which is applicable through synthetic jet, is much more demanding than the pulsating flow [28]. Therefore, based on aforementioned studies and their results, synthetic jet has been applied in this study to reduce the flow separation up until 33 %.

Related to the active flow control analysis, Chun et al. (1996) studied the introduction of the local forcing in the region near the separation edge in order of finding the relation between the forcing amplitude and the domain of the recirculation zone.

It was concluded that by utilizing this technique (localized perturbation near the separation edge), features of the separation and reattaching flows were altered significantly where by increasing the forcing amplitude, the recirculation length will be decreased significantly [29].

In studies related to the closed loop methods, more focus has been done over the synthetic jet as the actuator in the BFS geometry. Guo et al. (2017) conducted a numerical analysis to study the effect of applying the supersonic jet as an active flow control method in the hypersonic BFS geometry. The aim of this study was to compare the effect of the inserted jet where in one set of experiment it was vertically while in another, it was located horizontally. The result demonstrated that between the vertical location of the jet has less influence over the recirculation length while it has major effect in the boundary layer thickness. On the other hand, effect of the jet which has been placed horizontally showed the major influence over the recirculation length [30]. Dejoan and Leschziner (2014) investigated effect of applying the periodic perturbation stimulated by slot jet in the BFS geometry which has been introduced into the shear layer [7]. The schematic of the synthetic jet which has been applied in the active flow control methods is shown in the following Figure 1.5 [9].

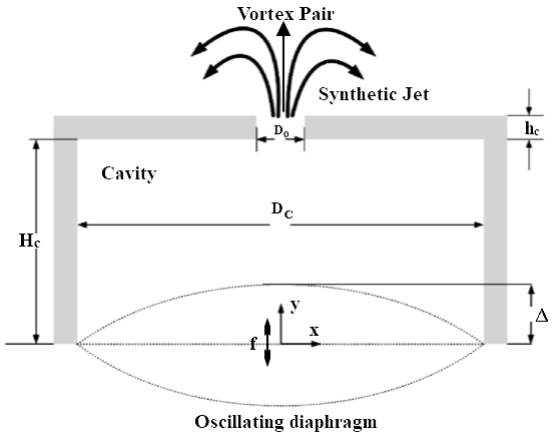

Figure 1.5 : Schematic of the oscillating-deforming diaphragm synthetic jet with cavity and orifice beneath a free stream [9].

In an analytical study conducted by Tang et al. (2006), a correlation for modeling the performance estimation of the circular synthetic jet were developed [14]. Based on the dimensional analysis which has been, it is concluded that U_{peak} can be defined independently as a proportion of the U_{max} which is the maximum of the main inlet velocity.

U_{peak} is the peak value of the main inlet velocity of the jet in sinusoidal synthetic jet. The outlet velocity of the jet based on U_{peak} can be calculated as shown in the following equation (1.3) .

$$u_o(t) = \frac{\dot{Q}_o(t)}{\rho A} = U_{peak}(t) sin(2\pi f t) \tag{1.3}$$

For the Computational Fluid Dynamics (CFD) analysis, inlet-velocity boundary condition was applied at the neutral position of the diaphragm instead of having dynamic boundary condition [12]. This decision has been made based on previous studies where this simplification had an insignificant effect on the velocity profile [31]. Due to considering the synthetic jet in the closed loop control method, review over the various applications of the adaptive PID controllers is necessary. Having nonlinearities and disturbances in the controlling of the dynamical systems, using artificial intelligence leads to have efficient decisions of the operator in the process. Zhao et al. (1993) examined the rule-based scheme of the fuzzy logic system for gain scheduling of the PID controller to apply in the SIMULINK model [18].

Shahzadi et al. (2016) applied the fuzzy logic with higher precision and performance to predict the output flow rate in simulating the straight microchannel. In this study, mamdani model has been considered in the designed fuzzy inference system with 3 membership functions for both input parameters including channel radius and applied pressure. Similarly, same number of the membership functions were considered for the flow rate of fluid as the output. The results indicated the error value of 0.47 % between the exact data of the experiments and the outputs of the designed fuzzy inference system [32]. Fuzzy logic controller has been applied for plant process control in the study by Pathmanathan et al, 2010. The aim was based on alternating the PID controller with fuzzy logic controller to regulate the amount of feed to reactor, amount of heating fluid leading to control the temperature of the product and the level of fluid in the tank. The results showed the better control performance, robustness and stability of the fuzzy controller over the PID controller based on having low value of Rising Time (RS), Settling Time (ST) even though there was negligible Overshoot (OS) for the fuzzy controller [17]. Since the manual tuning of these controllers is tedious which leads to their poor performance, more efficient way of applying the PID controllers with various techniques of optimization have been applied both in simple and fuzzy-PID controllers.

These optimization methods have been applied in order of reducing the negative step response characteristics including OS, ST and RT of the PID controllers through the procedure [33]. Two selected methods which have been considered for investigation in this era are GAO and PSO methods. GAO is the stochastic global search method operating based on natural selection and genetic principles which evolves with the number of iteration. Mantri and Kulkarni (2013) compared two tuning methods for the PID controller which has been implemented in the missile altitude controlling process in order of demonstrating their efficiency. The gains of the PID controller has been optimized based on GAO method and compared with the traditional Z-N tuning method. The results indicated that the optimized PID controller based on the GAO method has much faster response related to the classical method based on having less values for the RT and ST values [34]. Mirzal et al. (2012) investigated the effectiveness of the implemented GAO method in reducing the First Order Lag Plus time Delay (FOLPD) in the PID controller. The achieved results compared with other Iterative and Z-N tuning methods. In this study, it has been proven that the GAO method improved the FOLPD transient response by reducing the overshoot 70% and 30% percent in comparison with Z-N and Iterative procedures respectively. However, the value of RT and ST have shown the insignificant changes. Additionally, the trade off the genetic algorithm is the slightly reducing the stability of the system [35]. Chiou et al. (2012) designed the experiment based on finding the optimized PID controller based on PSO reinforcement evolutionary method to be utilized in the suspension system of the automobile industry as an active control method. In this approach by utilizing the Q-learning, individuals enhanced their own performance based on their social interactions and their private cognition. This optimization method, was applied in order of searching in high-dimensional space to find the appropriate membership function, rule set and the behavior of corresponding system. The results indicated that the revolutionized fuzzy-PID controller operates more efficiently and accurately for the considered system [36]. Specifically, suspension reflection, spunge mass acceleration and beating distance between the tire and the ground is reduced for the optimized fuzzy-PID controller in comparison with passive suspension syetem. Mahmud et al. (2011) investigated the PID controllers with gains which have been optimized during the simulation using the classical Z-N and the PSO algorithm methods to conduct

a comparison of their efficiency. The results concluded that the PSO based PID controller has the less value of OS compared to the Z-N based PID controller [37]. The same perspective is proved where Bassi et al. (2011) carried out a simulation to compare the effectiveness of the PSO algorithm in tuning the PID controller over the classical Z-N method. The outcome proved the easy implementation, stable convergence characteristics and good computational efficiency of the novel proposed method in the speed control of DC motor [33].

1.4 Objective of the Research

In the previous studies, despite of applying sinusoidal synthetic jets, any further modification in this specific active flow control method for the BFS system has not been conducted. Furthermore, previous studies have not investigated the effect of applying any type of PID controller in the BFS system as an active flow control method. Therefore, the novel idea based on utilizing the PID contoller to adapt the velocity of the sinusoidal synthetic jet is proposed to reduce the recirculation length and drag coefficient more effectively. However, previous studies proved the lack of performance in the conventional PID controllers. Consequently, the concept of applying fuzzy-PID controller which has been optimized using the GAO and PSO methods is proposed in this thesis as well. In order of accomplishing this tasks, a SIMULINK model with BFS geometry was studied numerically in which a sinusoidal synthetic jet at the step wall was applied. The velocity of this specific jet is set by utilizing the optimized fuzzy-PID controller.

2. PROBLEM DESCRIPTION

The core idea of the present study is to optimize the fuzzy-PID controller using GAO and PSO methods. Afterwards, the optimized fuzzy-PID controller is applied over the sinusoidal synthetic jet in the BFS geometry to investigate the more reduction of the reattachment length with respect to the BFS case without aforementioned jet. Regarding the defined goal, in section 3, the primary simulations has been done in order of validating and verifying the cases of studies for both without-jet and with-jet based on previous similar studies. For the case of without considering jet, the numerical simulation was validated based on Armaly et al, 1983 [26]. For the case of applying jet, the study which was carried out by Coskun et al. (2021) has been applied [27]. Afterwards, the simulation based on considering sinusoidal jet was conducted. After reaching the desirable agreement between the conducted numerical analysis and the aforementioned basis references, the main analysis which includes the sinusoidal synthetic jet in the middle of the step in order of creating the sinusoidal continuous blowing and suction force flows has been conducted. The simulations were conducted in the laminar flow domain in three different Reynolds number as 200, 300 and 400. In order of having active control over the simulation procedure, the PID controller has been applied. This was proceeded by designing a SIMULINK model in which the extracted transfer function from CFD analysis has be considered in the first step. The transfer function was extracted from the data of the simulation related to the Re=400. The validation of the transfer function was carried out based on Re=200 and Re=300. After finding the desirable transfer function, SIMULINK analysis was conducted based on considering three different PID controllers including the conventional, fuzzy and optimized fuzzy PID controllers. Based on author's knowledge, there have not been studies related to the velocity control of the sinusoidal synthetic jet based on optimized fuzzy-PID controllers so far. Two methods of optimizations including GAO and PSO have been defined based on least step response characteristic values (OS, RT and ST) of the fuzzy-PID controller at least possible time accompanied with system stability. The parameters which has been optimized were the index of the membership functions

of the outputs, the domain of the applied membership functions of the input and outputs and the coefficients (K_1, K_2 and K_3). After reaching the optimized values for the aforementioned inputs parameters, the optimized fuzzy-PID controller was compared with normal and fuzzy-PID controllers. The optimized fuzzy-PID controller was applied in the SIMULINK model where instead of applying the transfer function, ANSYS FLUENT software was coupled with MATLAB utilizing the written function and the simulation process was carried on.

In section 4 (Result and discussion), the validation results for with and without jet cases were demonstrated. Results of the optimization procedure was elaborated for finding the best way of optimization with least value of cost function and Number of the Function Evaluation (NFE). After that, the comparison between three applied PID controllers have been conducted. Finally, outcomes of applying the optimized fuzzy-PID controller over the drag coefficient has been demonstrated and the comparison between the cases of applied optimized fuzzy-PID controller and without PID controller was conducted.

3. MATERIALS AND METHODS

3.1 Numerical Study

The procedure which has been followed sequentially in the numerical computations includes governing equations, computational domain, boundary conditions, numerical solution procedure and characteristics calculations. These steps are described in more details in following sections.

3.1.1 Governing equation

For both with and without jet cases of studies, in the Cartesian coordinate system, the continuity and Navier-Stokes have been written based on following equations (3.1) and (3.2) for mass and momentum conservation respectively. In studies where the heat transfer analysis was considered, energy equation was applied as well.

$$\frac{\partial \rho}{\partial t} = \nabla.(\rho \vec{U}) = 0 \tag{3.1}$$

$$\frac{\partial \rho \vec{U}}{\partial t} + \nabla(\rho \vec{U}\vec{U}) = -\nabla P + \mu \nabla^2 \vec{U} \tag{3.2}$$

3.1.2 Computational domain and boundary conditions

The considered computational domains and boundary conditions for the case of study are demonstrated in Figure 3.1. The domain length of the entrance region before the step which has been named Back Wall (BW) in Figure 3.1, is L_{BW}=0.04 m. The height of the entrance region and the step are selected h_i=0.01 m and h_s=0.01 m respectively. The domain after the step which has been named Front Wall (BW) in Figure 3.1, is selected L_{FW}=0.3 m. Based on aforementioned values and equation (1.1), the dimensionless ER parameter is calculated 2 for this analysis. This details are shown in Table 3.1 as well.

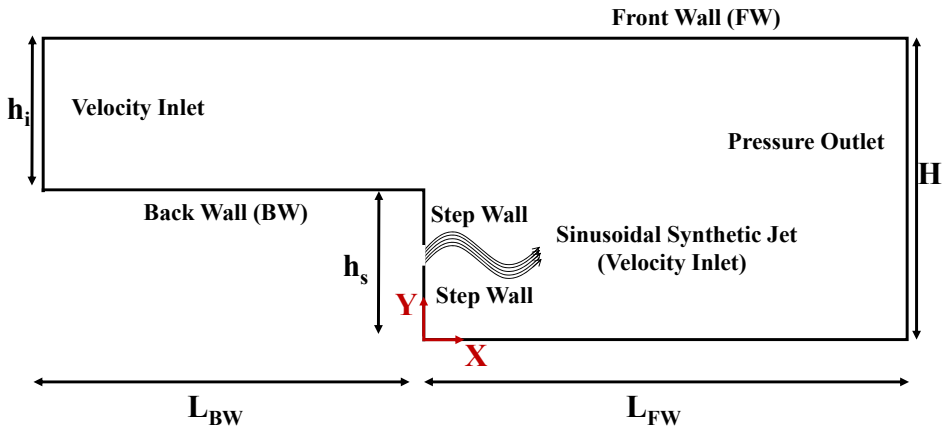

Figure 3.1 : Schematic of the considered geometry for sinusoidal synthetic jet case.

Table 3.1 : Names and values of the domains in the cases of study.

Names of domains	Values of domains [m]
L_{BW}	0.04
L_{FW}	0.3
h_{i}	0.01
h_{s}	0.01

Velocity profile was defined based on parabolic correlation as demonstrated in equation (3.3) for the inlet of the domain.

$$u(y) = -4 \times U_{\infty}[(\frac{y}{h})^2 - \frac{y}{h}] \tag{3.3}$$

In which U_{∞}=0.4506 ms^{-1} which is equivalent to Re=400. Velocity inlet and pressure outlet boundary conditions are defined for the inlet and outlet of the geometry respectively. All other edges of the domain including at the top, bottom and back of the step are selected as wall boundary conditions [26, 27].

Additionally, for the velocity profile of sinusoidal synthetic jet, the frequency was considered 20 Hz [38]. The peak magnitude of the jet velocity (amplitude: $\mathrm{U_{peak}}$) for the simulation is applied based on the average main inlet velocity of the flow (U_{avg}= (2/3) $\times U_{\infty}$) [38]. Therefore, the correlation which has been applied for the sinusoidal jet velocity is defined based on following equation (3.4).

$$U_{\mathrm{peak}} = (\frac{2}{3}) \times U_{\mathrm{max}} \times sin(2\pi t) \tag{3.4}$$

The boundary condition for the considered jet in this simulation was defined as a "velocity inlet" boundary conditions [27].

3.1.3 Numerical solution procedure

The simulation for the considered aforementioned cases were carried out as following. Since the simulation was conducted in the laminar domain, the viscous (laminar) model has been considered. Due to having the fluctuation of flow in the fluid domain caused by applied jet, the simulation was conducted in unsteady situation in the laminar flow domain for Re=200, Re=300, and Re=400. Since the simulation was conducted in unsteady situation, PISO algorithm with Least Square Cell for coupling the pressure-velocity was considered. Second order Upwind accuracy for spatial discretization of pressure and momentum were defined and second order implicit for the time were applied. Both of parabolic and sinusoidal velocity profiles were interpreted into ANSYS FLUENT using User Defined Function. The applied fluid was air in which viscosity and density were 1.81e-5 Nsm^{-2} and 1.205 Kgm^{-3} respectively. The simulation was continued up until 1.5 second time period where the 0.0005-time step was considered.

3.1.4 Characteristic calculations

For this case of study, the skin friction and drag coefficients along the bottom wall after the step were selected as the criteria of the aerodynamic performance. The skin friction and drag coefficients are calculated via equation (3.5) and equation (3.6) respectively.

$$C_{f,x} = \frac{\tau_w}{\frac{1}{2}\rho U_\infty^2} \tag{3.5}$$

$$C_D = \frac{F_D}{\frac{1}{2}\rho U_\infty^2 A} \tag{3.6}$$

3.1.5 Validation and verification

Two cases of validation have been considered in our study. For the validation of the "without-jet" case, the experiment conducted by Armaly et al. (1983) in 389 Reynolds number was considered. Velocity profiles at different location along the bottom wall after the step and the value of the reattachment length in the experiment were extracted in order of making comparison with numerical data from the conducted simulations [26]. The study by Coskun et al. (2021) was considered for the validation of the "with jet" case of study.

The variation of the skin friction coefficient along the bottom wall after the step for two configurations of [2 -1 -1] and [0 -2 2] were compared with the CFD simulations [27]. The schematic of the computational domain and boundary conditions for both cases of validation have been shown in Figure 3.2 and Figure 3.3 for cases of without and with jet respectively.

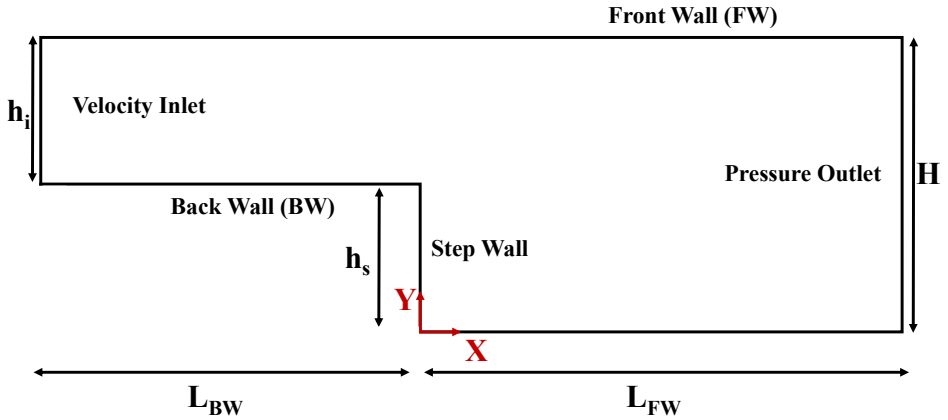

Figure 3.2 : Schematic of the considered geometry for without-jet case inspired by Armaly et al, 1983 [26].

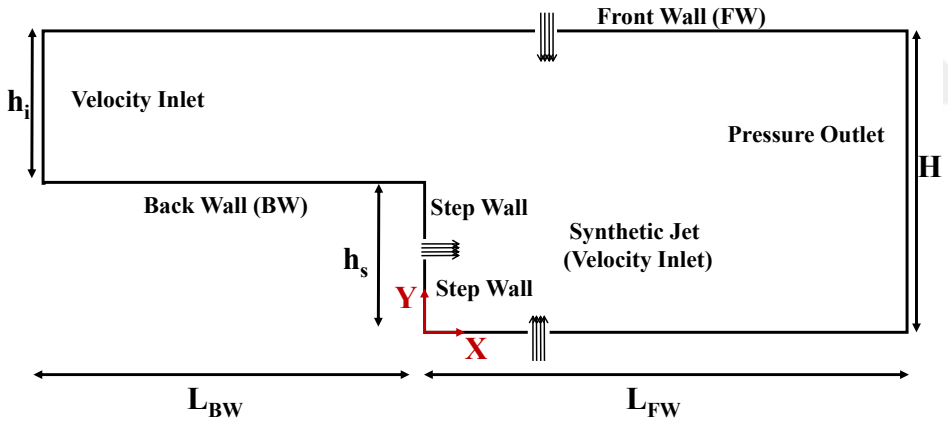

Figure 3.3 : Schematic of the considered geometry for with-jet case inspired by Coskun et al, 2021 [27].

3.1.6 Mesh independency

The criterion which has been considered for mesh independency is the recirculation length [26]. Five different mesh sizes were considered where the mesh with minimum number of cells and acceptable accuracy in recirculation length value would be applied in the simulation procedure. Table 3.2 represents the number of cells for each edge defined in the domain of the geometry.

Figure 3.4 depicts the defined edges in the selected 3rd mesh design for the numerical analysis.

Table 3.2 : Considered mesh sizes for mesh independency [without jet].

Mesh Design	VI	BW	FW	SW	NC
1st	24	99	749	24	40128
2nd	49	199	1499	49	160253
3rd	59	239	1799	59	230703
4th	79	319	2399	79	410003
5th	99	399	2999	99	640503

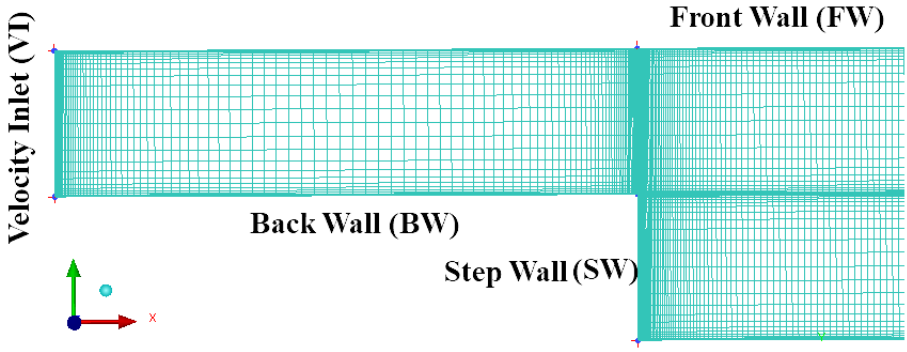

Figure 3.4 : Schematic of the considered geometry for without-jet case.

For the case of considering jet, the study done by Coskun et al. (2021) was considered since the same geometry with same computational domain will be applied for the case of considering sinusoidal synthetic jet. The considered criterion was recirculation length. Five different mesh sizes as described in Table 3.3 were investigated. The mesh with minimum number of cells with acceptable accuracy of the recirculation length would be chosen [27]. The selected 3rd mesh design for CFD analysis with the defined edges is shown in Figure 3.5.

Table 3.3 : Considered mesh designs for mesh independency [with jet].

Mesh Design	VI	BW	FMW	FEW	SW	Jet	NC
1st	30	108	29	525	15	8	38879.00
2nd	33	108	31	525	15	8	41011.00
3rd	61	184	58	1179	29	12	169222.0
4th	100	400	99	2900	49	36	736861.0
5th	130	400	149	2900	74	36	1006891

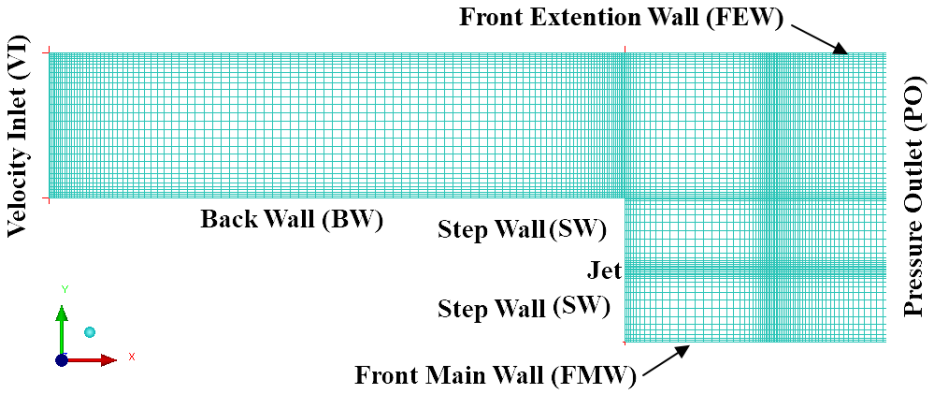

Figure 3.5 : Schematic of the considered geometry for with-jet case.

3.1.7 Time independency

In the with-jet case of study, the time independency was proceeded in order of reaching the desirable time step value. The time independency would be studied for the 3rd mesh design in which the minimum value of the Δx was 0.07 cm. Therefore, the Courant number (CFL) has been calculated based on following equation (3.7).

$$CFL = U_{max}\Delta t/\Delta x \tag{3.7}$$

Since CFL should be less than one, therefore, threshold value of one was considered. In order of reaching the defined value, δt was calculated as follows having in mind that U_{max} was 0.4506 ms^{-1} for Re=400.

$$CFL \leq 1 \rightarrow \Delta x/U_{max} = 1 \rightarrow \Delta t \leq 0.0016 \tag{3.8}$$

From above correlation, 0.0016 second was achieved as the maximum value for time step. After that, 0.0015 s, 0.001 s, 0.0005 s and 0.0001 s were considered for the time independency investigation.

3.2 Transfer Function

Since direct connection between MATLAB and FLUENT in order of finding the optimized fuzzy-PID controller would be expensive, the transfer function has been considered in the optimization process. After conducting the simulation for three cases including the Re=200, Re=300 and Re=400 in laminar flow domain, values of the jet velocity and drag coefficient at peak of each the sinusoidal period were imported as the input and output for the systemIdentification Toolbox of MATLAB (Figure 3.6) to reach the desirable transfer function.

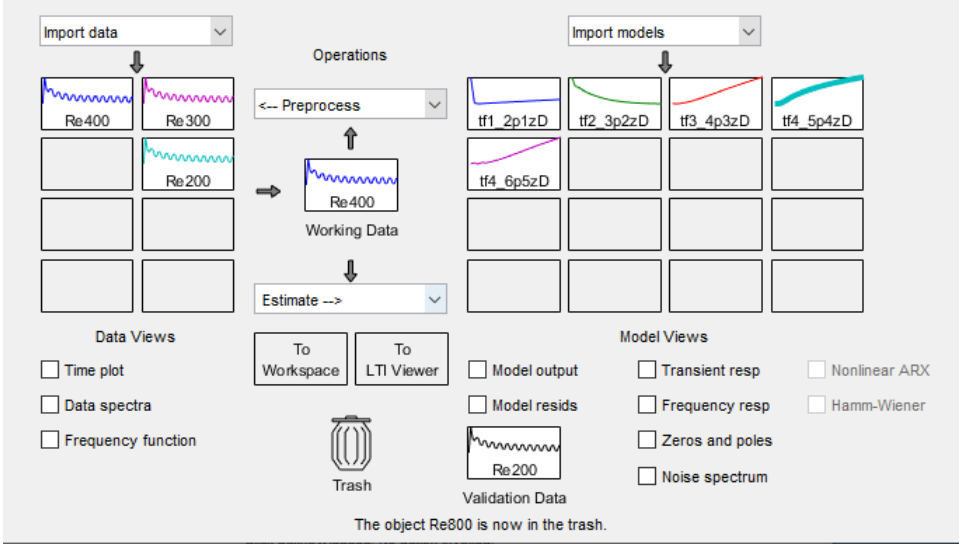

Figure 3.6 : SystemIdentification Toolbox for extracting the transfer function.

Since the data at the peak of the sinusoidal pattern have been gathered from the simulation data set, therefore, discrete transfer function was considered in this process. Due to applying the frequency of 20 Hz, by considering the following equation (3.9), the 0.0125-time step was considered for gathering the data and applying them in systemIdentification Toolbox.

$$sin(2\pi \times 20t) = 1 \rightarrow 40t = \frac{\pi}{2} \rightarrow t = \frac{1}{80} = 0.0125 \tag{3.9}$$

After comparing various discrete transfer functions with different poles and zeros as shown in Figure 3.7, the transfer function with 5 poles and 4 zeros was reached the highest accuracy regarding the gathered simulated data from CFD analysis and considered in the pre-simulation of the model in SIMULINK as the transfer function.

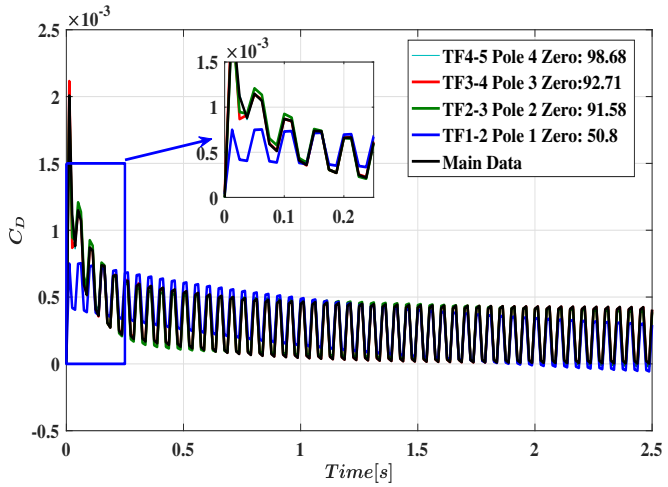

Figure 3.7 : Comparison of various configurations of zeros and poles.

Equation (3.10) is the correlation of the desired transfer function which would be considered in this optimization process. Data from Re=200 and Re=300 will be evaluated by on this transfer function for validating the performance of the transfer function.

$$TF = \frac{5.8e-5z^2+0.001352z^3-0.0001378^2-0.001049z}{z^5-3.03z^4+3.286z^3-1.509z^2+0.2838z-0.03066} \tag{3.10}$$

3.3 PID Controller

After reaching the desired transfer function, SIMULINK model for the PID controller was designed. For each transfer function, there is an ultimate gain (K_u) where in this value, the system starts oscillating and becomes unstable. In other word, K_u is the point that stands between the stable and unstable conditions. Consequently, there will be T_u which is the oscillation period, meaning the time period between two oscillations. In other word, T_u is the period of the system which occurs at the edge of the stable and unstable conditions. At the beginning, the gains of the PID controller including K_p (proportional gain), K_i (integral gain) and K_d (derivative gain) were tuned using classical Z-N method based on K_u and T_u [16]. The values of the K_u and T_u were 22.0992 and 0.031252 which have been calculated through written code in MATLAB.

$$K_p = 0.6K_u \tag{3.11}$$

$$K_i = 1.2\frac{K_u}{T_u} = \frac{K_p}{T_{\mathrm{u}}} \tag{3.12}$$

$$K_d = 0.075\frac{K_u}{T_u} = \frac{K_pT_u}{8} \tag{3.13}$$

By finding the aforementioned values, the tuning of the PID was conducted. Based on aforementioned configurations, the related SIMULINK model was designed which is demonstrated in the following Figure 3.8.

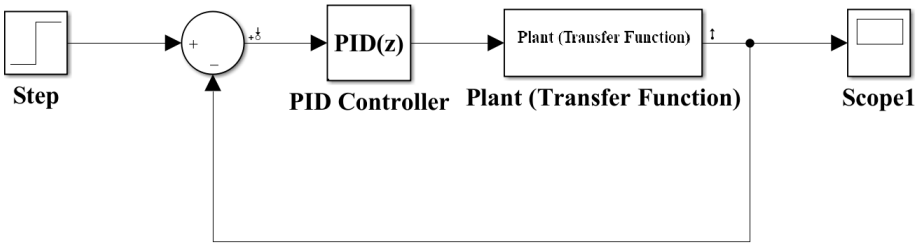

Figure 3.8 : Schematic of the designed PID controller in SIMULINK.

3.4 Fuzzy-PID Controller

In order of having fuzzy-PID controller, the fuzzy inference system based on Zhao et al. (1993) designed in order of applying over the PID controller in the SIMULINK model [18]. Due to applying normalized values of outputs for the fuzzy-PID, normalized values of the outputs based on following equations (3.14) and (3.15) for K_p and K_d were defined respectively.

$$K_p^{'} = \frac{K_p - K_{p,min}}{K_{p,max} - K_{p,min}} \tag{3.14}$$

$$K_d^{'} = \frac{K_d - K_{d,min}}{K_{d,max} - K_{d,min}} \tag{3.15}$$

Instead of considering the K_i, α has been defined in order of having more concentration on two gains of fuzzy-PID controller rather than three for saving computation time [18]. It can be proven that K_i can be calculated based on K_p and K_d as shown in equations (3.16) and (3.17).

$$T_d = \frac{K_d}{K_p} \tag{3.16}$$

$$T_i = \frac{K_p}{K_i} \tag{3.17}$$

T_i and T_d are integration and derivative times respectively. Therefore, the relation between the α, K_i, K_d and K_p can be indicated in equation (3.18).

$$\alpha = \frac{T_i}{T_d} = \frac{K_p}{K_i} \times \frac{K_p}{K_d} = \frac{K_p^2}{K_i \times K_d} \rightarrow \alpha = \frac{K_p^2}{K_i \times K_d} \tag{3.18}$$

$$K_i = \frac{K_p^2}{\alpha K_d} \tag{3.19}$$

Fuzzy Inference System (FIS) was coded in MATLAB based on considering the inputs including the error and derivative of error while outputs include normalized proportional ($K_p^{'}$), differential ($K_d^{'}$) gains and α (implying integral gain ($K_i^{'}$)) of the PID controller. The considered rules between inputs and outputs of this designed FIS has been originated from the study done by Zhao et al, 1993 [18]. Centroid and bisector defuzzification methods were considered in this research. Triangular and gaussian membership functions were considered for the defined inputs and outputs. Mamdani fuzzy inference system has been implemented in this study for the implication purpose.

For this model, the output membership functions are in a distributed form for proportional and derivative gains while it is semi-singleton membership function for the α to enhance the defuzzification process due to its constancy and simplicity and consequently higher efficiency [39]. All other details of the designed FIS are summarized in Table 3.4.

Table 3.4 : Properties of the designed FIS.

Components of structure	Detail
Inference system	Mamdani
Membership function	Triangular/Gaussian
Implication method	Mamdani-min
Inputs	error, derivative of error ($\dot{e}$)
Outputs	$K_p{}'$, $K_d{}'$, α
fuzzy operator	And-min
Aggregation method	Max
Defuzzification method	Centroid-Bisector
Rule weight	1

In the designed the FIS, due to having two inputs and three outputs, variation of each output parameter can be depicted based on two input parameters. Therefore, Figure 3.9 to Figure 3.11 demonstrate the three dimensional plots of each output with respect to inputs. The shape of variation of the aforementioned plots has been related to the domain of the inputs and output parameters and additionally, the defined rules of the FIS. The rules of the designed FIS have been selected based on the conducted study by Zhao et al, 1993 [18].

In a FIS, instead of having crisp values for inputs and outputs, domains of the parameters is divided in memberships. This is the core idea of having flexibility in a FIS [18]. Figure 3.12 to Figure 3.16 show the domains and names of the membership functions for the inputs (error and derivative of error) and outputs ($K_p{}'$, $K_d{}'$ and α) of the FIS without applying any optimization methods being proposed by Zhao et al, 1993 [18]. Figure 3.12 and Figure 3.13 shows that error and derivative of error, as the inputs of the FIS, have been divided into seven triangular membership functions. The names which has been assigned for these membership functions from left to right are Negative Big (NB), Negative Medium (NM), Negative Small (NS), Zero (ZO), Positive Small (PS), Positive Medium (PM), Positive Big (PB).

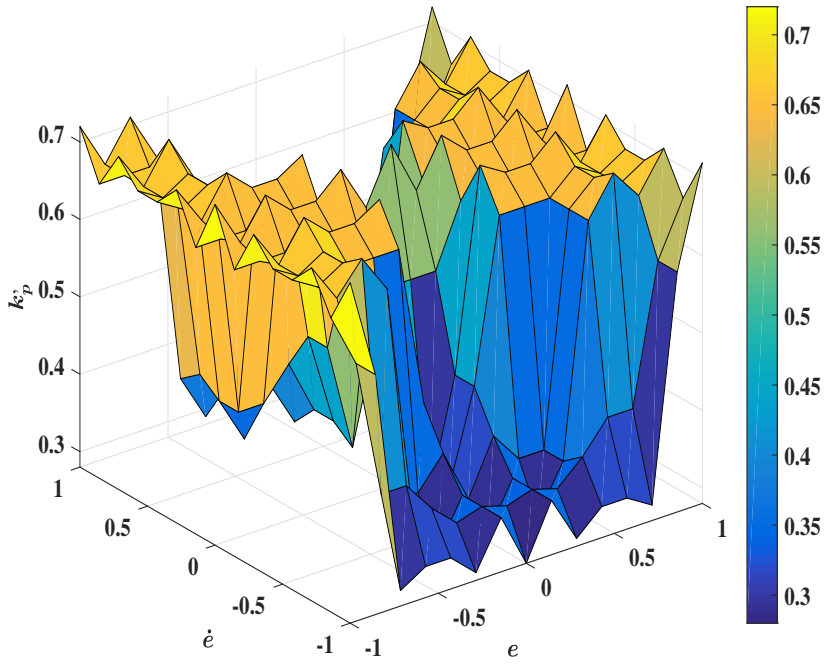

Figure 3.9 : Variation of $K_p{}'$ with respect to error and derivative of error in FIS.

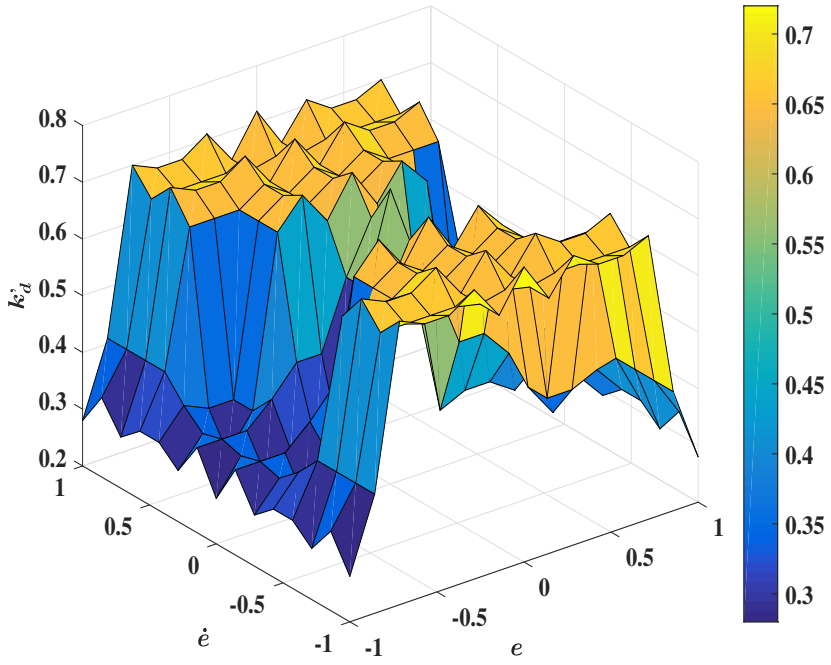

Figure 3.10 : Variation of $K_d{}'$ with respect to error and derivative of error in FIS.

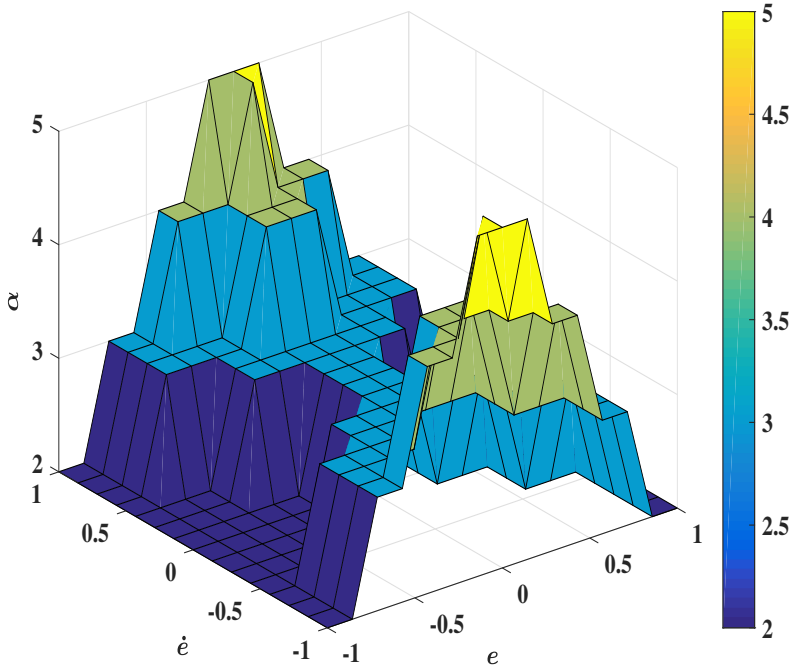

Figure 3.11 : Variation of α with respect to error and derivative of error in FIS.

As depicted in Figure 3.14 and Figure 3.15, for $K_p{}'$ and $K_d{}'$, two gaussian membership functions have been selected. The names which have been assigned for them are Small and Big from left to right. Since the normalized value of these gains have been considered in the FIS, the domain of them is between zero and one. The standard deviation of the gaussian membership functions for both of these normalized gains have been selected 0.427. The considered mean value for the first and second membership function of these normalized outputs are zero and one respectively.

For third output, (α), four values of 2, 3, 4 and 5 have been considered. In order of applying this memberships into the FIS, for each of the selected crisp values, four triangular membership functions have been defined. The feet values for each of these triangular membership functions have been selected 0.05. This strategy is shown in Figure 3.16. After designing the FIS, SIMULINK model based on fuzzy-PID controller was designed in which proportional, derivative and integral gains were updated in each time step based on constructed FIS and this process continued up until the considered time to reach the defined value in the step point block. Schematic of the designed fuzzy-PID controller in the SIMULINK model has been shown in Figure 3.17.

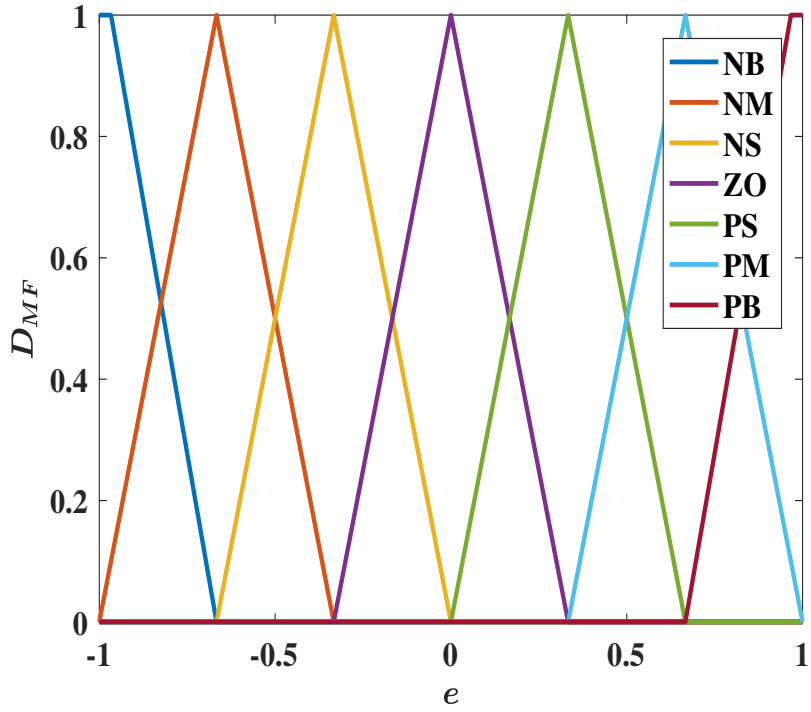

Figure 3.12 : Membership function distribution of error.

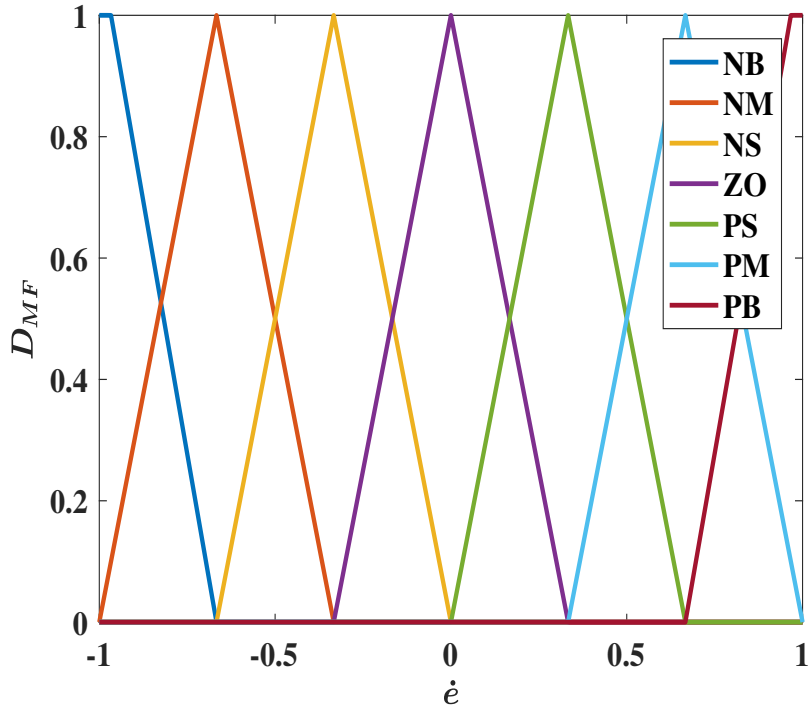

Figure 3.13 : Membership function distribution of derivative of error.

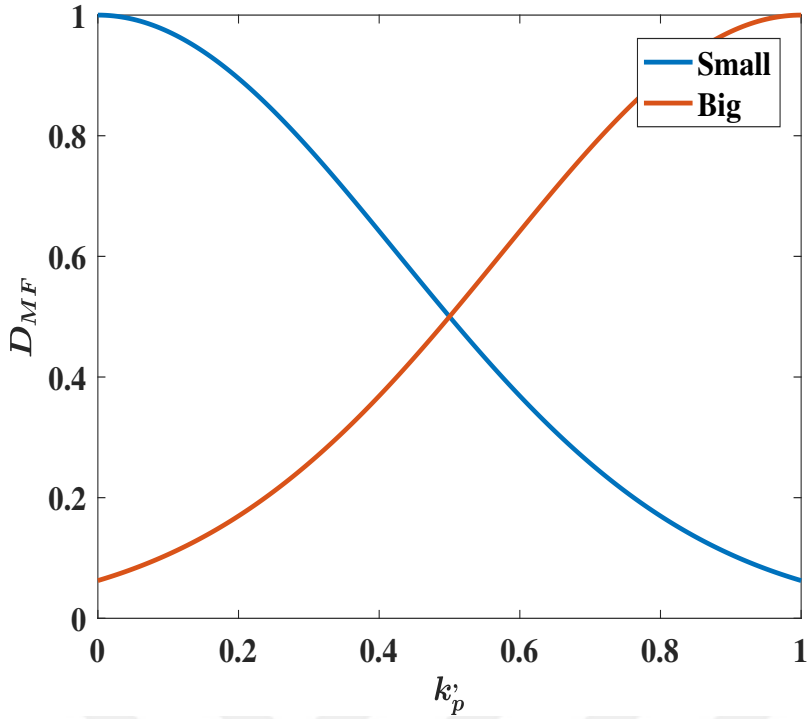

Figure 3.14 : Membership function distribution of $K_p{}'$.

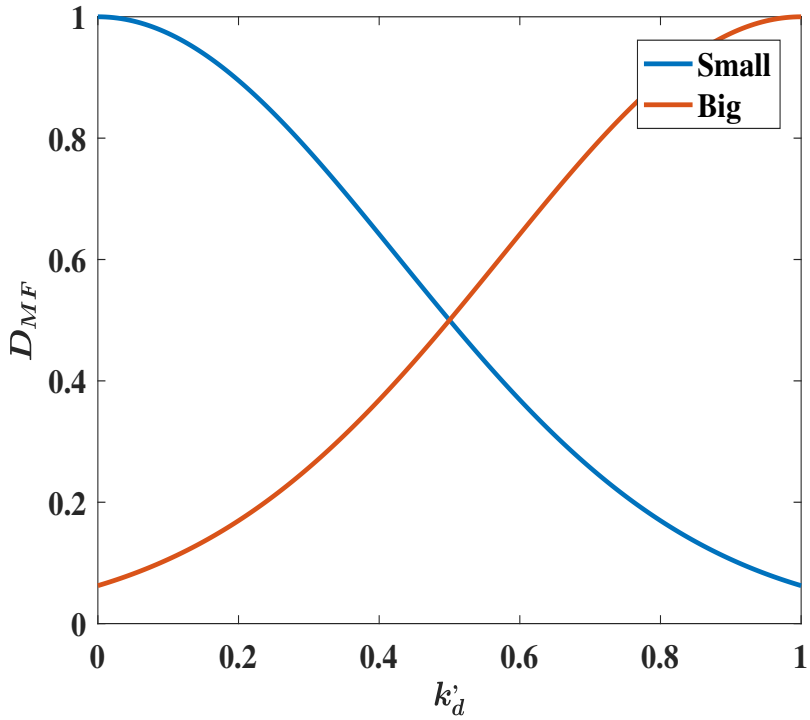

Figure 3.15 : Membership function distribution of $K_d{}'$.

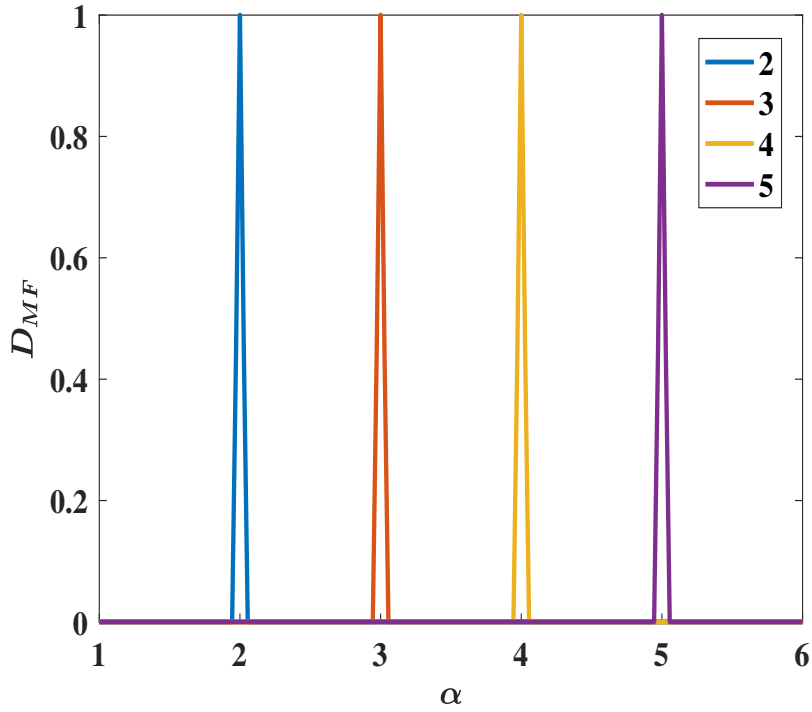

Figure 3.16 : Membership function distribution of α.

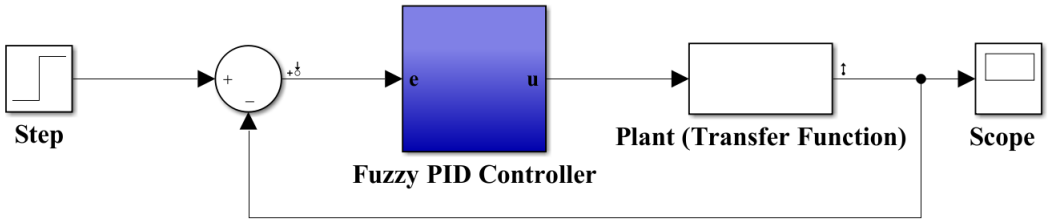

Figure 3.17 : Schematic of the fuzzy-PID controller designed in the SIMULINK.

Detailed schematic of the constructed fuzzy-PID controller is depicted in Figure 3.18. As it be can be seen, error and derivative of error are imported as inputs and the gains of the PID controller are outputs of the FIS including K_p, K_d and α (K_i). The outputs of the FIS were imported to the function to reach the real (Not-Normalized) values of gains. To compare the step response of the fuzzy and conventional PID controllers, the following SIMULINK model was designed as shown in Figure 3.19.

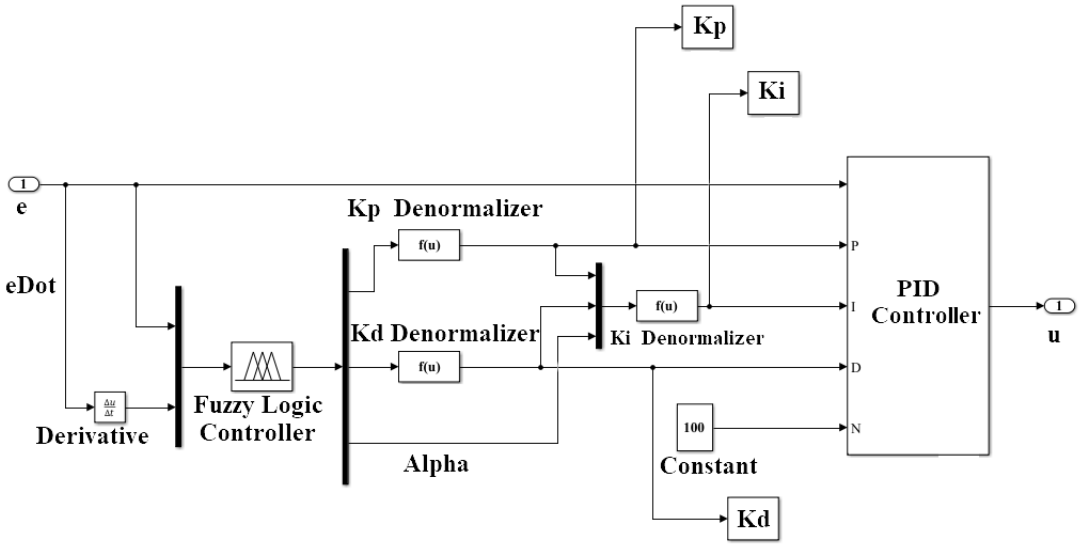

Figure 3.18 : Schematic of the fuzzy-PID controller.

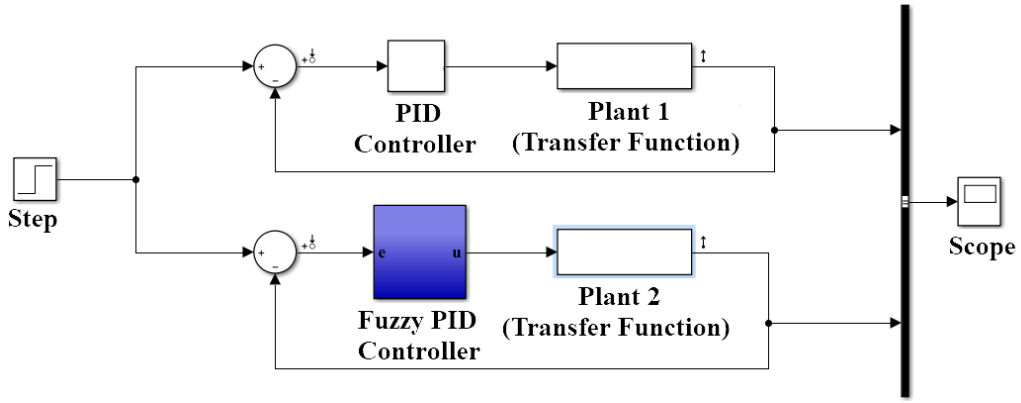

Figure 3.19 : Schematic of the comparison design between the normal and fuzzy-PID controller in SIMULINK.

The initial values for the $K_{p,min}$, $K_{p,max}$, $K_{d,min}$ and $K_{d,max}$ have been calculated based on equations (3.20) to (3.23) respectively [18]. These initial values have been imported in all designed SIMULINK models.

$$K_{p,min} = 0.32K_u \tag{3.20}$$

$$K_{p,max} = 0.6K_u \tag{3.21}$$

$$K_{d,min} = 0.08K_uT_u \tag{3.22}$$

$$K_{d,max} = 0.15K_uT_u \tag{3.23}$$

3.5 Optimized fuzzy-PID Controller

Due to aiming for reducing the step response characteristics of the fuzzy-PID controller which are OS, ST and RT, two optimization algorithms including GAO and PSO methods were applied. The parameters which have been optimized are the domain of the applied membership functions of inputs and outputs, the index of the membership functions of outputs assigned in the rules definition and the stabilizing coefficients (K_1, K_2 and $K_{p,min}$). The range of the constituents (OS, ST and RT) included in the cost function is not same and therefore, normalizing process should be done. Following equation (3.24) has been applied for this purpose [40].

$$F_i^{norm}(x) = \frac{F_i(x) - F_i^{min}}{F_i^{min}} \tag{3.24}$$

In the above equation, $F_i(x)$ represents the individual constituents of the total cost function. The total cost function is defined based on equation (3.25).

$$CF_{norm} = W_1 OS_{norm} + W_2 RT_{norm} + W_3 ST_{norm} \tag{3.25}$$

3.5.1 Genetic algorithm

In the process of the genetic algorithm, there are different steps. The first step is creating the initial population. The population of inputs have been created based on considered boundaries and initial values in the written code of MATLAB. After conducting the initial evaluation of the population, the crossover and mutation have been carried out based on calculated probabilities. In general, there are three methods of selecting individuals for crossover including random selection (RS), roulette wheel selection (RWS) and tournament selection (TS). Random selection method is the method without considering the cost function criterion. However, in roulette wheel and tournament selections, choosing individuals have been conducted based on the probability related to their cost function (or rank). In the final step, all three populations (initial, mutated, and crossed over) have merged and sorted based based on cost function criterion. In the next step, truncation based on the limited number of population size has been applied and finally, by reaching the considered criterion, the algorithm will be stopped. The whole process can be demonstrated in the following flowchart of the algorithm in Figure 3.20.

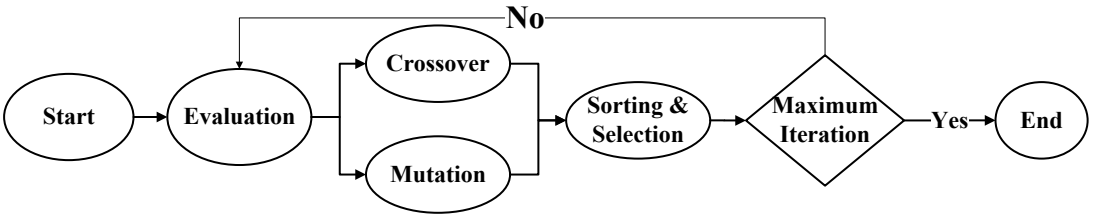

Figure 3.20 : General schematic of the Genetic Algorithm.

3.5.2 Particle swarm optimization method

Particle Swarm Optimization (PSO) known as searching process based on swarm intelligence includes individuals named particles defined as the potential solution of the optimized N dimensional search space with capability of storing the optimal position of the swarm. Figure 3.21 represents the procedure of the PSO algorithm.

The optimization of the fuzzy-PID controller by considering the two aforementioned optimization methods were conducted. Based on achieved results for three designed PID controllers, the optimized fuzzy-PID controller were investigated and compared in the SIMULINK model as shown in Figure 3.22.

3.6 Coupling FLUENT and SIMULINK

By finding the best configuration of the optimization method for the fuzzy-PID controller, the desired optimized fuzzy-PID controller has been applied in the SIMULINK model where the FLUENT software has been coupled and considered in the plant section of the model. The schematic of the model has been demonstrated in the following Figure 3.23.

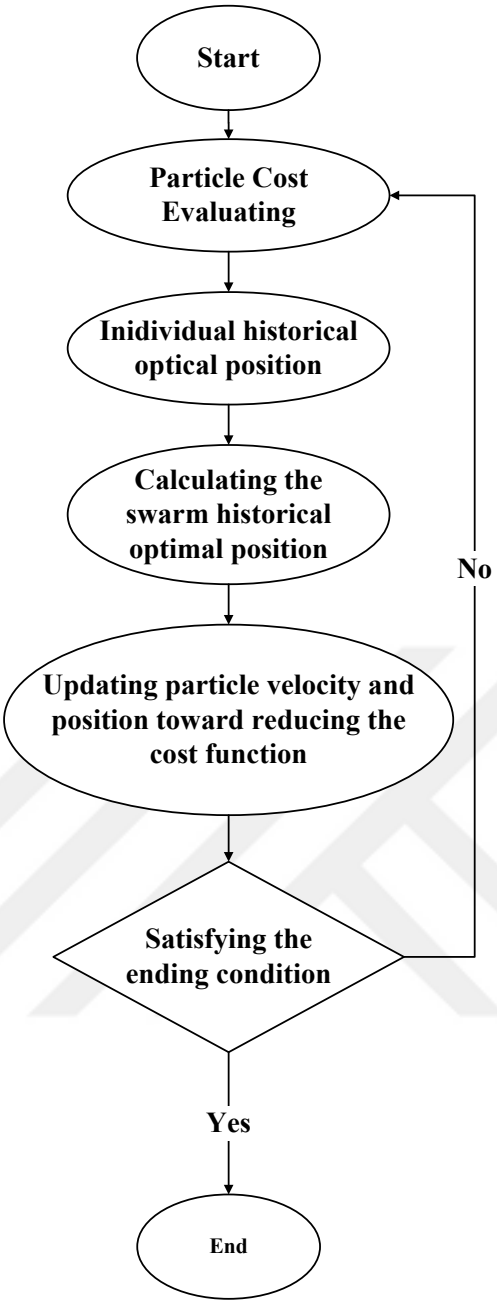

Figure 3.21 : Procedure of the Particle Swarm Optimization.

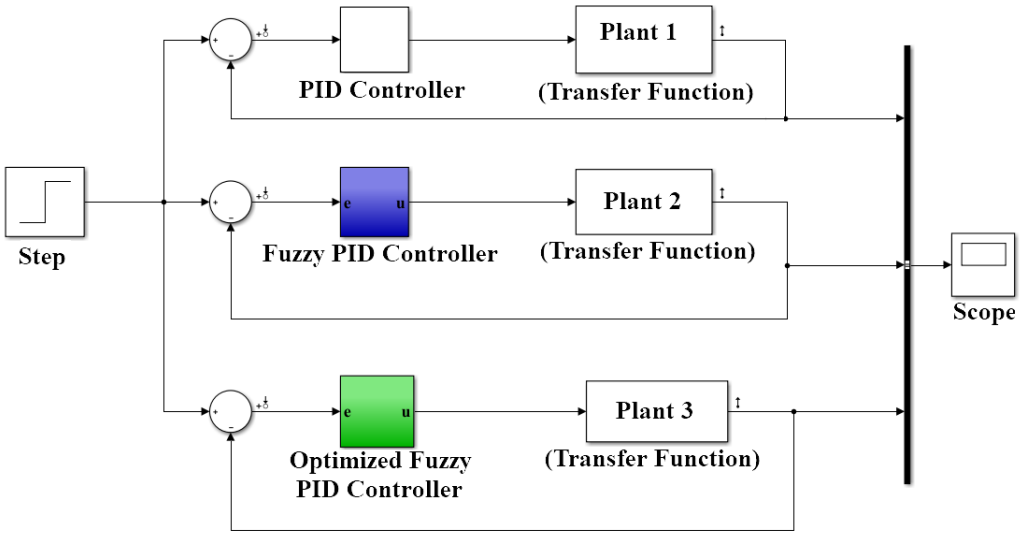

Figure 3.22 : Schematic of the considered SIMULINK model for comparison of three considered PID's.

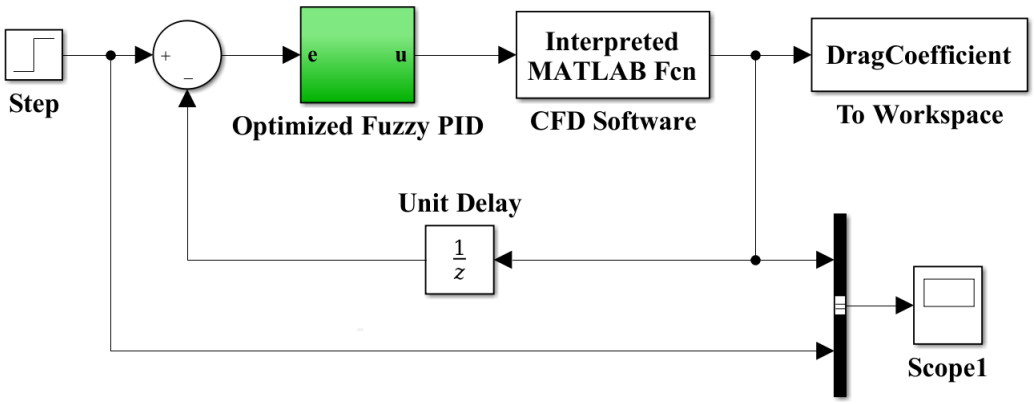

Figure 3.23 : Schematic of the SIMULINK model coupled with FLUENT.

4. RESULT AND DISCUSSION

4.1 Validation and Verification

4.1.1 Without jet

The result of the mesh independency which was conducted for the without-jet case is demonstrated in Figure 4.1. It can be seen after the 3rd mesh design, the variation of the considered parameter is negligible. Therefore, this mesh design was considered for upcoming simulations.

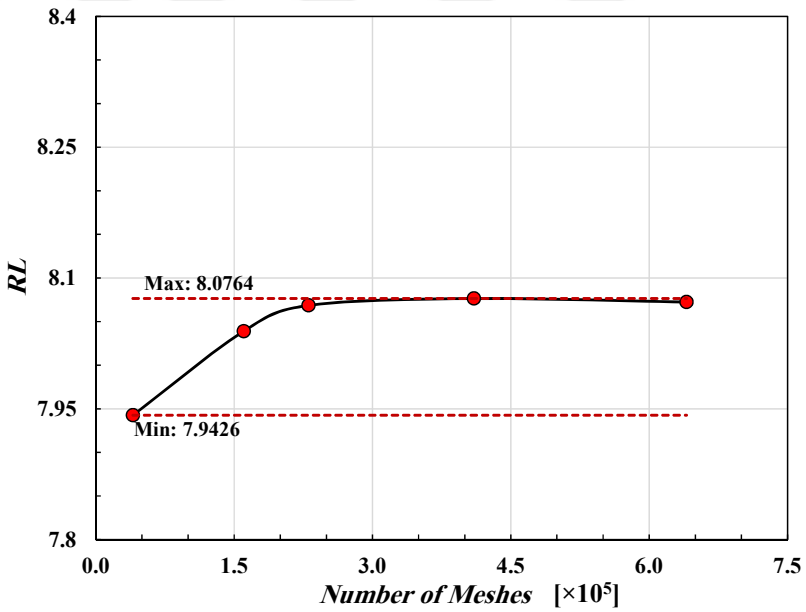

Figure 4.1 : Mesh independency for case without Jet.

Validation was conducted based on the study done by Armaly et al, 1983. The velocity profiles in relative distances from the step wall were compared with the numerical analysis. Figure 4.2 to Figure 4.8 demonstrate the comparison of the present study and experimental data. It can be concluded that there is a good agreement with the basis study done by Armaly et al, 1983 [26]. The velocity profiles before the step wall imply the parabolic equation which had been applied in the velocity inlet boundary condition.

However, after the step, the negative values of the velocity imply the existence of the recirculation zone. Figure 4.2 illustrates the velocity profile upstream of the step. This figure shows that the accuracy of the conducted numerical analysis is acceptable. However, the more agreement can be seen in the middle of the inlet section rather than boundaries. Figure 4.3 represents the velocity profile after the step at X/h_s =2.55.

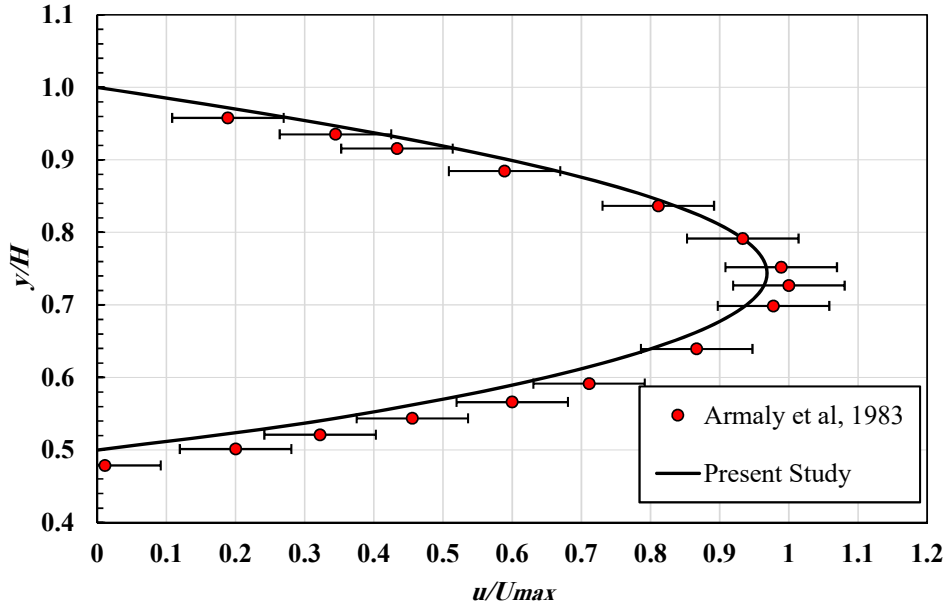

Figure 4.2 : Comparison of the experimental and numerical data at x/h_s=0 (Error bar=± 10%).

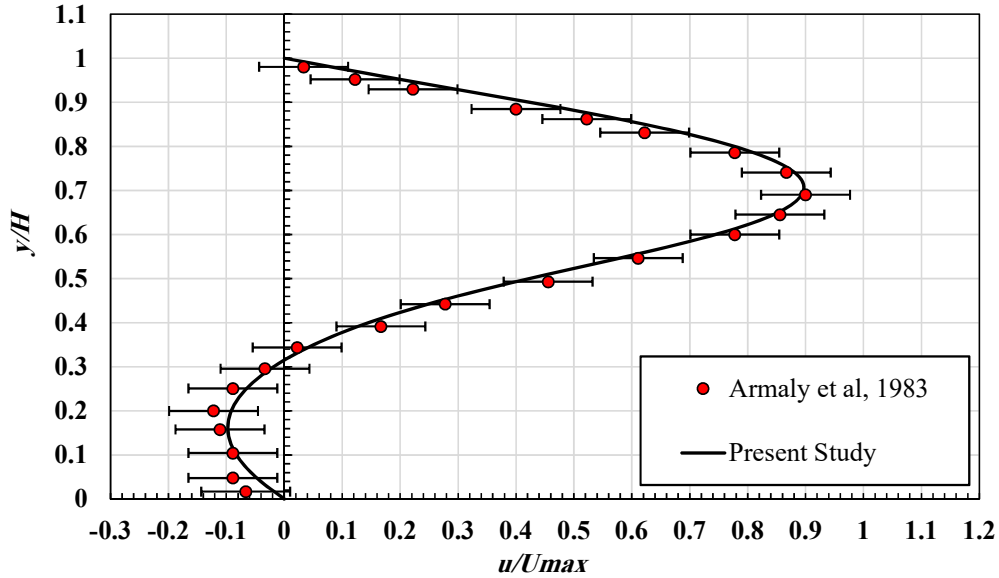

Figure 4.3 : Comparison of the experimental and numerical data at x/h_s=2.55 (Error bar=± 10%).

As it can be seen in the Figure 4.3, there is a good agreement both above and in the recirculation region after the step. Figure 4.4 represents the velocity profile after the step at X/h_s =3.06. The agreement achieved above the step and in the recirculation region are both acceptable and are in the range of 10%.

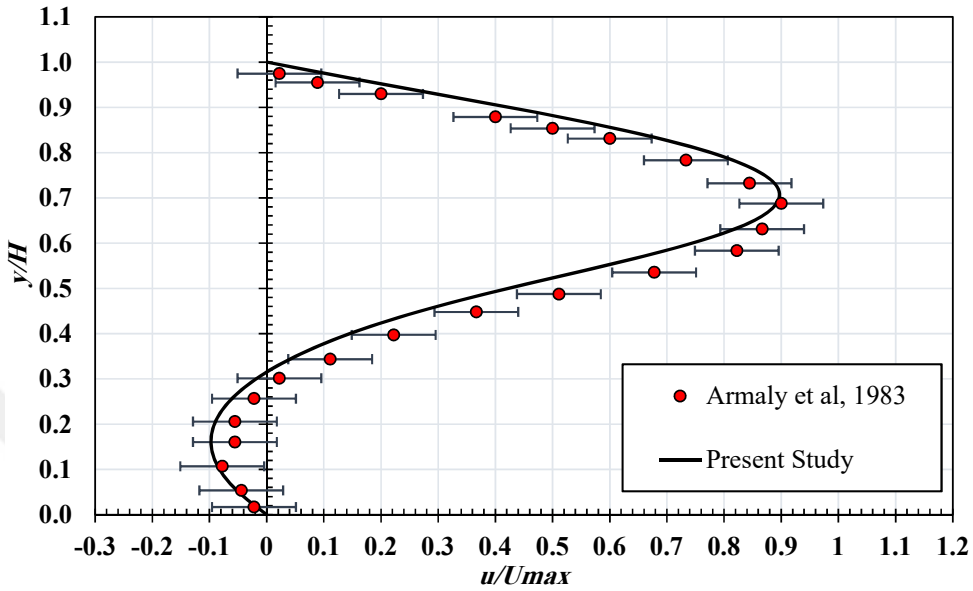

Figure 4.4 : Comparison of the experimental and numerical data at x/h_s=3.06 (Error bar=± 10%).

Figure 4.5 represents the velocity profile after the step at X/h_s =4.8. The good agreement has been achieved both above and in the recirculation region.

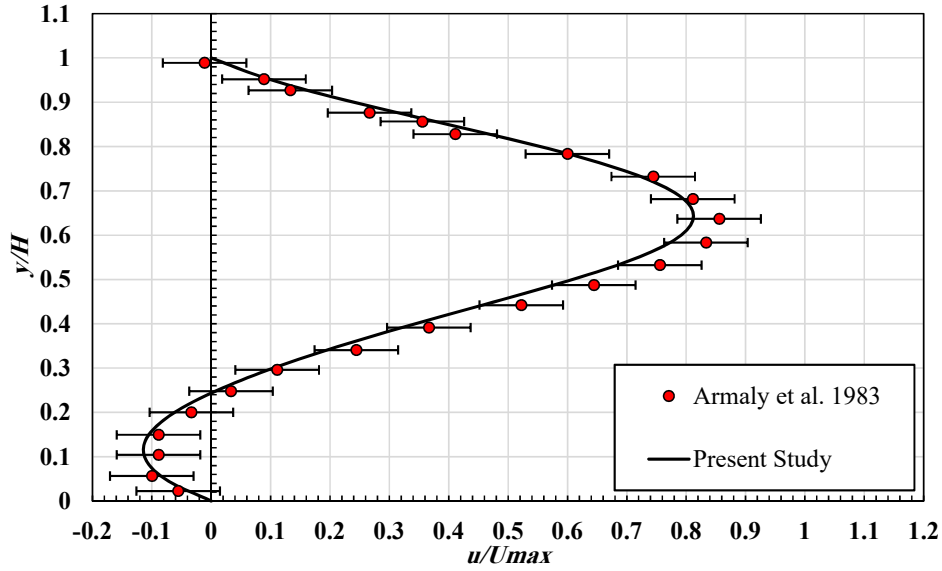

Figure 4.5 : Comparison of the experimental and numerical data at x/h_s=4.8 (Error bar=± 10%).

Figure 4.6 represents the velocity profile after the step at X/h_s =7.14. This figure depicts the good agreement with the experimental analysis for above and in the recirculation region. Based on the Figure 4.3 to Figure 4.6, it can be stated that the accuracy of the numerical data is better in the middle and end of the recirculation region than in the beginning of the recirculation region.

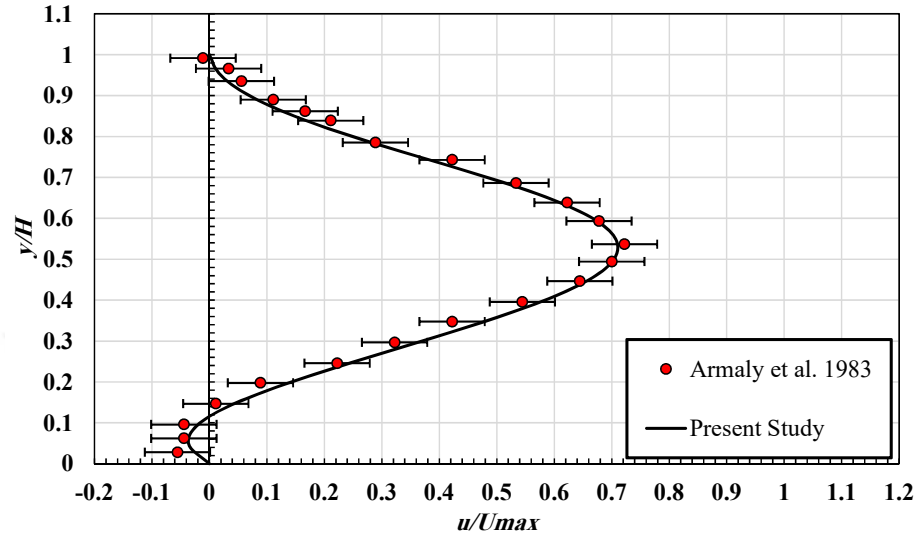

Figure 4.6 : Comparison of the experimental and numerical data at x/h_s=7.14 (Error bar=± 10%).

Figure 4.7 represents the velocity profile after the step at X/h_s =9.18. This figure depicts the better agreement for lower region than the upper region where it can be noticed that the recirculation region has been gone.

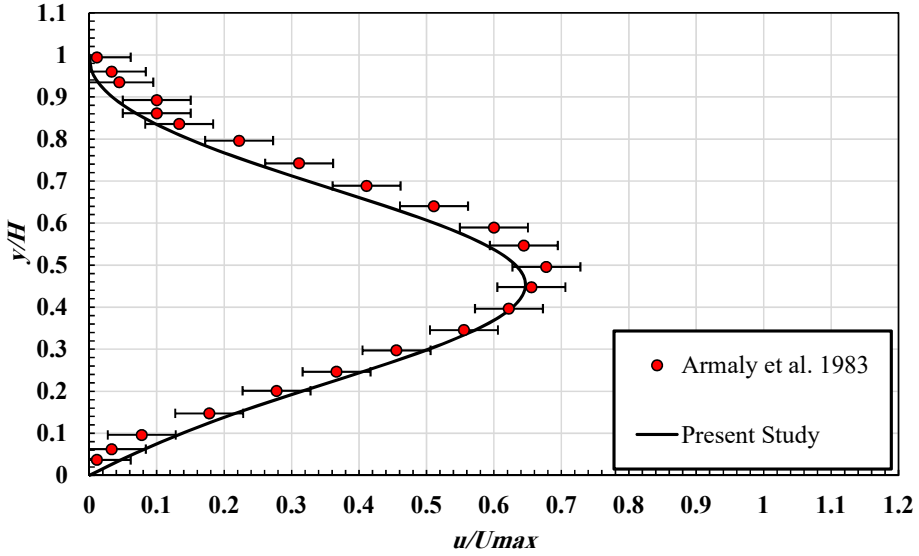

Figure 4.7 : Comparison of the experimental and numerical data at x/h_s=9.18 (Error bar=± 10%).

Figure 4.8 represents the velocity profile after the step at X/h_s =13.57. The good agreement both for lower and upper regions of the domain has been achieved.

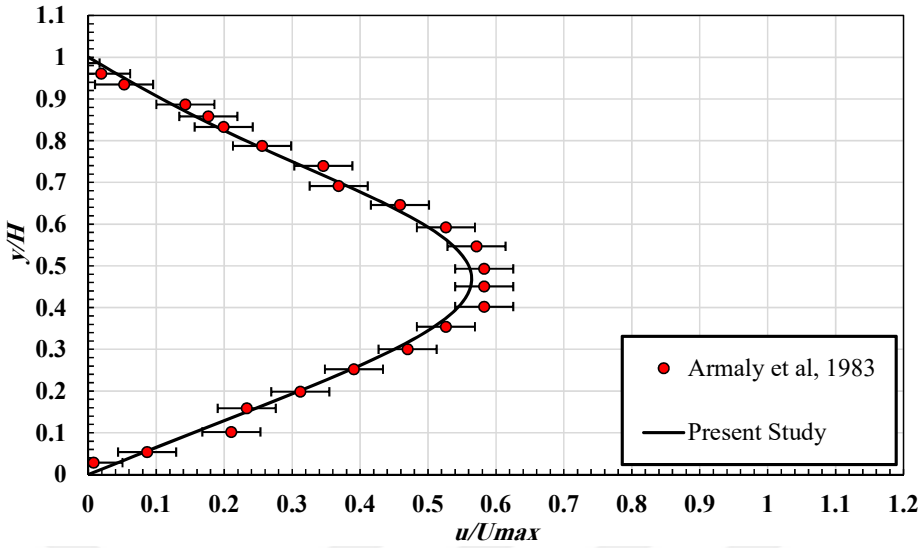

Figure 4.8 : Comparison of the experimental and numerical data at x/h_s=13.57 (Error bar=± 10%).

It can be understood from the Figure 4.6 and Figure 4.7 that the recirculation length has been ended between the x/h_s=7.76 and x/h_s=9.18 since the reverse domain of the velocity has been eliminated.

4.1.2 With jet

The results of the mesh independency for the with-jet case was demonstrated in Figure 4.9.

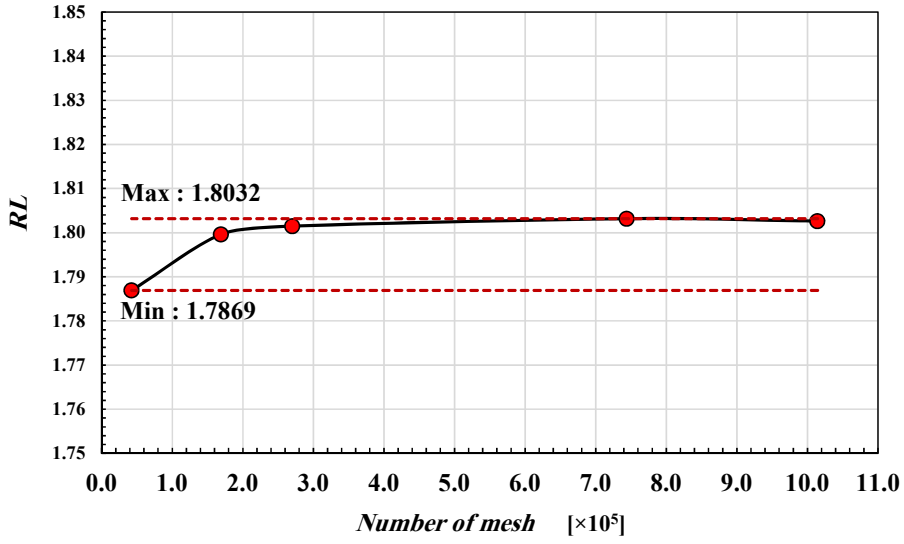

Figure 4.9 : Mesh independency for the case with jet criteria.

Since after the 3rd designed mesh, the variation of the considered parameter is negligible, this mesh was considered as the basis for upcoming CFD analyses.

Time independency analysis has been shown in Figure 4.10. It can be concluded from the figure, after the value of 0.0005 *s*, there is an insignificant difference in the defined criterion. Therefore, this value was considered as the desirable time step value for numerical analysis.

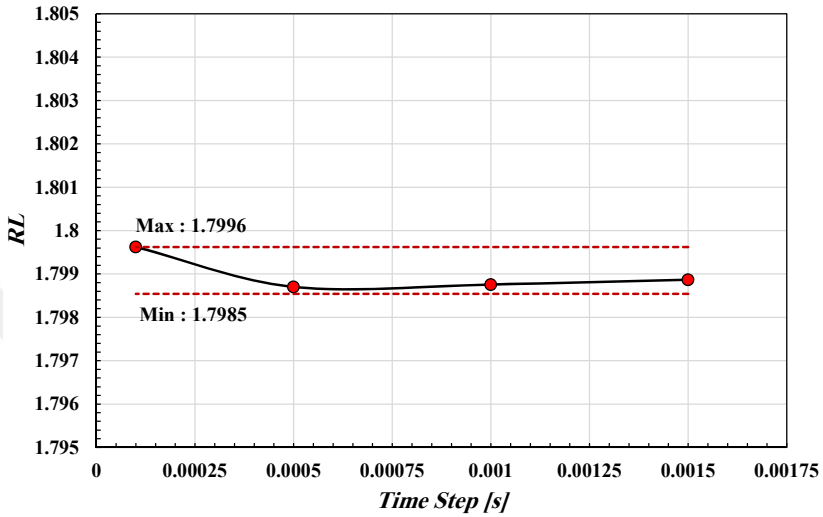

Figure 4.10 : Time independency for the case with jet criteria.

The results of comparison between numerical analyses with the work done by Coskun et al. (2021) have been shown in Figure 4.11 and 4.12 for [0 -2 2] and [2 -1 -1] cases of study respectively.

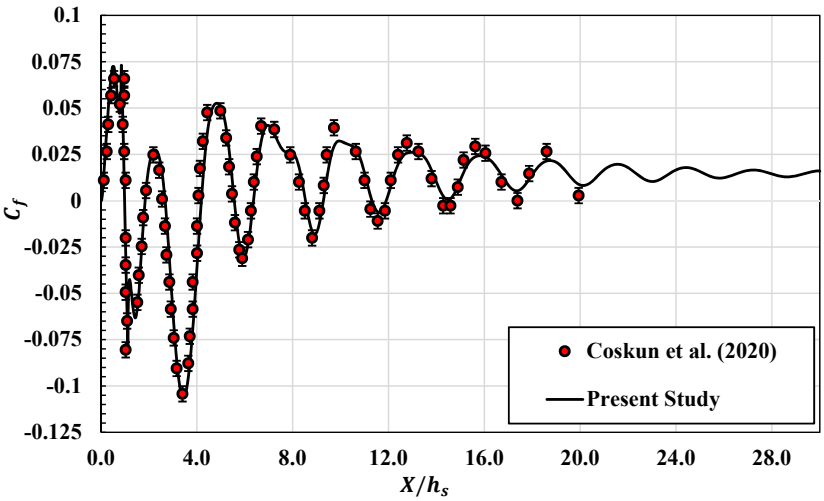

Figure 4.11 : Validation of the case [0 -2 2] with Coskun et al, 2021 [27] (Error bar=± 10).

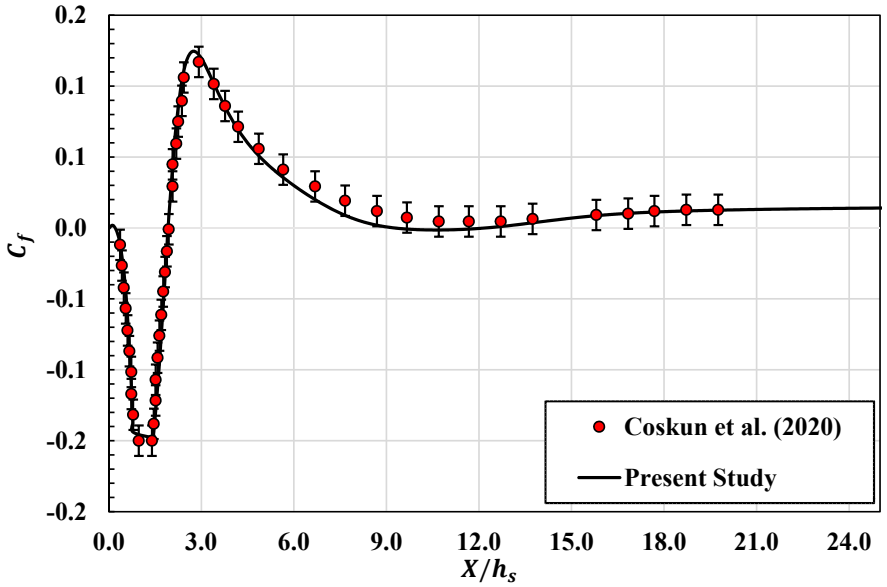

Figure 4.12 : Validation of the case [2 -1 -1] with Coskun et al, 2021 [27] (Error bar=± 10).

4.2 Performance of the Transfer Function

Figure 4.13 to Figure 4.15 demonstrate the validation cases which have been conducted by considering Re=200, Re=300 and Re=400 for the achieved transfer function.

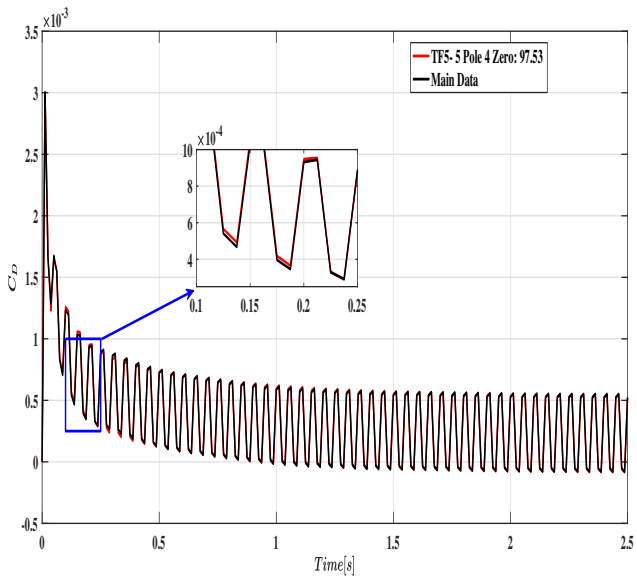

Figure 4.13 : Estimation of the simulated data of the Re=200 using the desired transfer function.

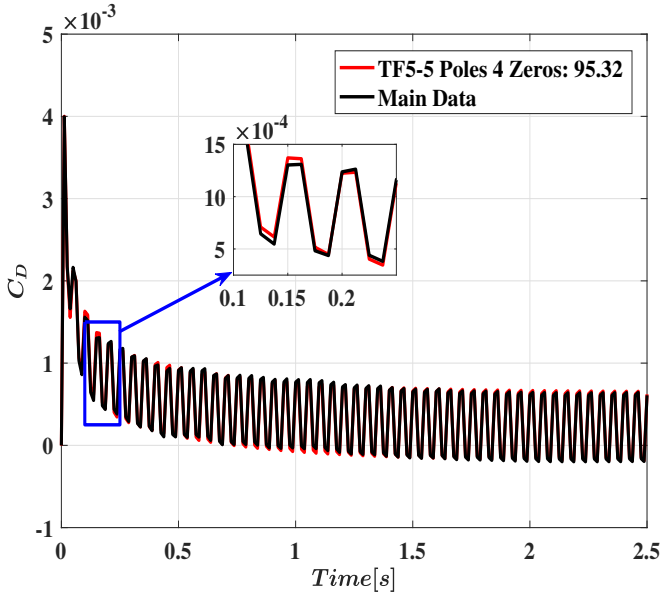

Figure 4.14 : Estimation of the simulated data of the Re=300 using the desired transfer function.

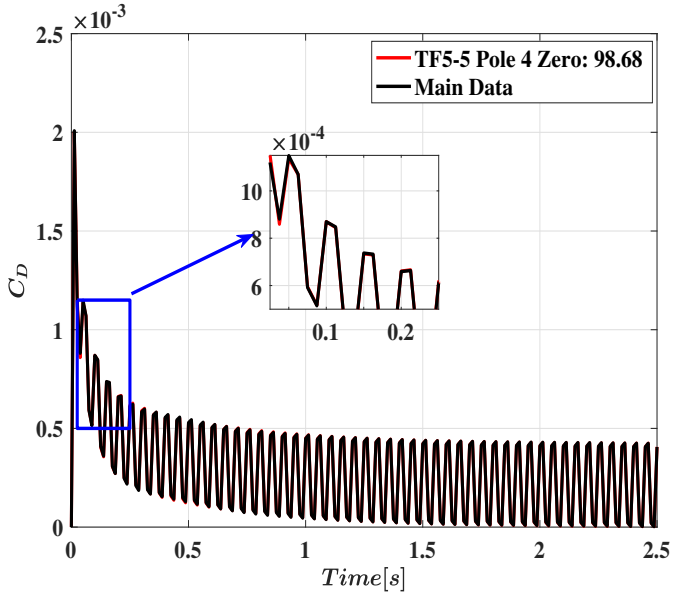

Figure 4.15 : Estimation of the simulated data of the Re=400 using the desired transfer function.

4.3 Conventional and Fuzzy-PID Controllers

Figure 4.16 depicts the step response comparison of the system for normal and fuzzy-PID controllers. This comparison demonstrates that OS, ST and RT have been decreased for the fuzzy-PID controller with respect to the PID controller.

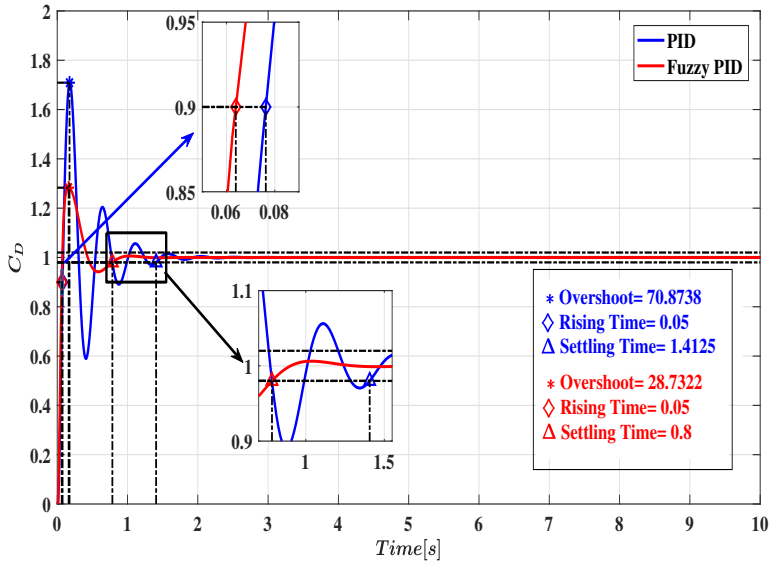

Figure 4.16 : Comparison of the step response of the conventional and fuzzy-PID controller.

4.4 Optimized Fuzzy-PID Controller

The designed FIS was optimized through GAO and PSO methods. Table 4.1 listed the constituent of the cost function (OS, RT and ST) in addition to the Number of the Function Evaluation (NFE) which is another considered criterion in evaluating the applied optimization methods. It can be resulted that GAO method by applying the Bisector defuzzification and TS method reached the least value of the cost function and NFE. Therefore, the FIS from this optimization method was extracted for upcoming investigations.

Table 4.1 : Comparison of the various applied optimization method.

Method	Deffuz		Iteration	NFE	OS	RT	ST	CF
GAO								
	Bisector	RS	84	5604	30.739	0.025	0.45	1.503
		RWS	198	13128	30.608	0.025	0.45	1.4992
		TS	44	2964	30.4397	0.025	0.45	1.4925
	Centroid	RS	66	4416	30.573	0.025	0.45	1.517
		RWS	141	9366	30.300	0.025	0.45	1.506
		TS	199	13194	31.922	0.025	0.45	1.572
PSO								
	Bisector		173	10440	61.358	0.0125	0.4375	1.683
	Centroid		186	11220	61.325	0.0125	0.4375	1.6251

Figure 4.17 to Figure 4.19 demonstrates the variation of $K_p{}'$, $K_d{}'$ and α regarding the assumed inputs respectively. Comparison between Figure 3.9 and Figure 4.17 depicts that the optimization process has affected the variation of the $K_p{}'$ in the path to reach the best efficient step response characteristics.

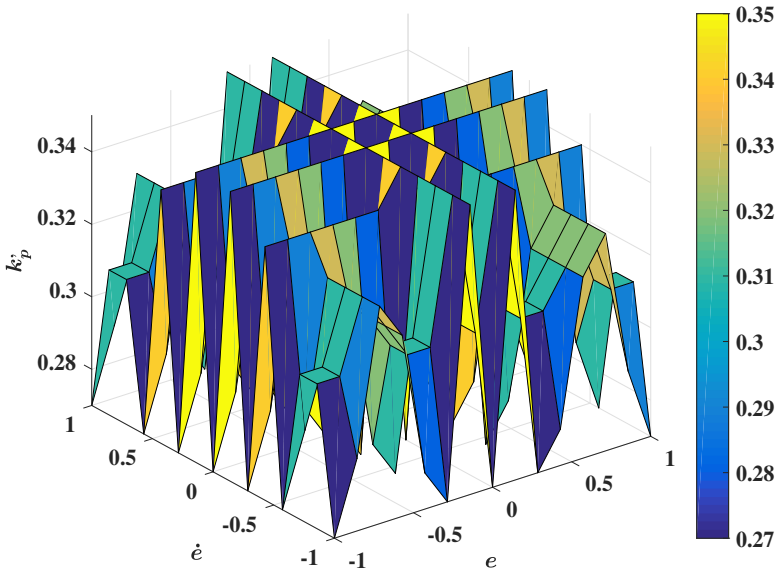

Figure 4.17 : Variation of $K_p{}'$ with respect to error and derivative of error in optimized FIS.

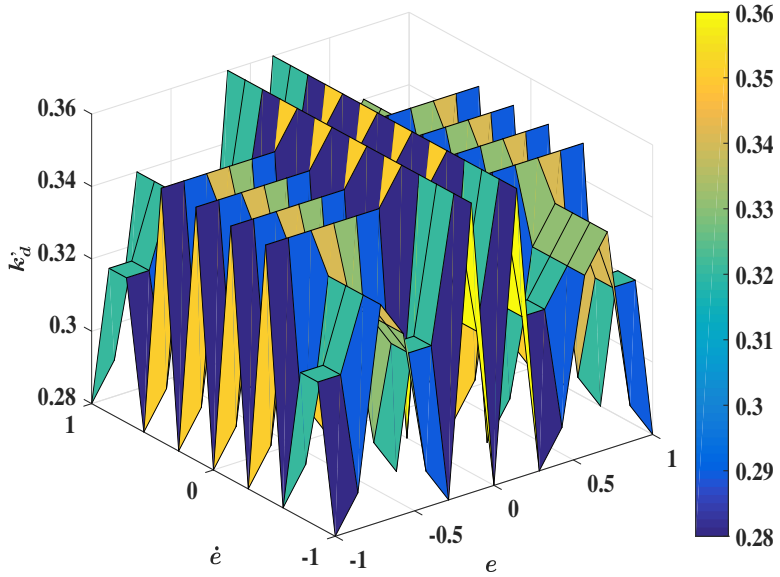

Figure 4.18 : Variation of $K_d{}'$ with respect to error and derivative of error in optimized FIS.

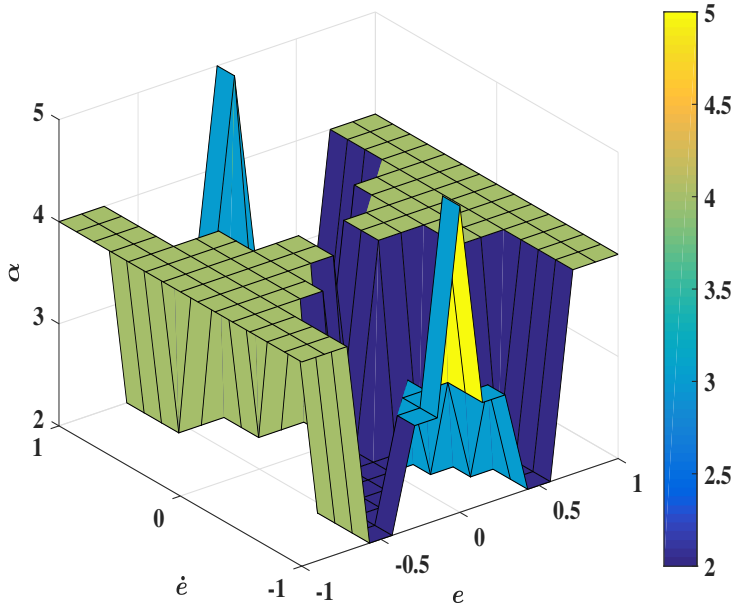

Figure 4.19 : Variation of α with respect to error and derivative of error in optimized FIS.

Similarly, the comparison of Figure 3.10 with Figure 4.18 and Figure 3.11 with Figure 4.19 represent the effect of optimization over $K_d{}'$ and α respectively. The domain modification of the degree of the membership functions has been shown in Figure 4.20 to Figure 4.24 for inputs (e and $\dot{e}$) and outputs ($K_p{}'$, $K_d{}'$ and α).

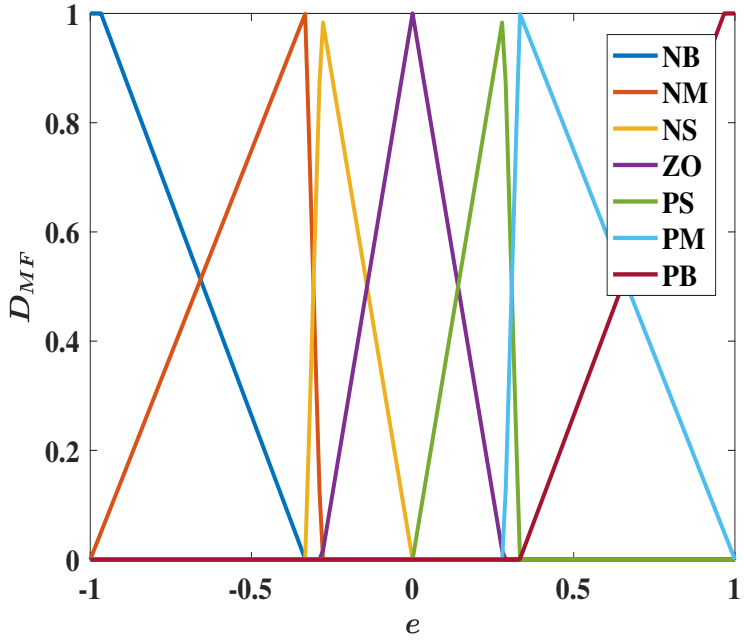

Figure 4.20 : Membership function distribution of error.

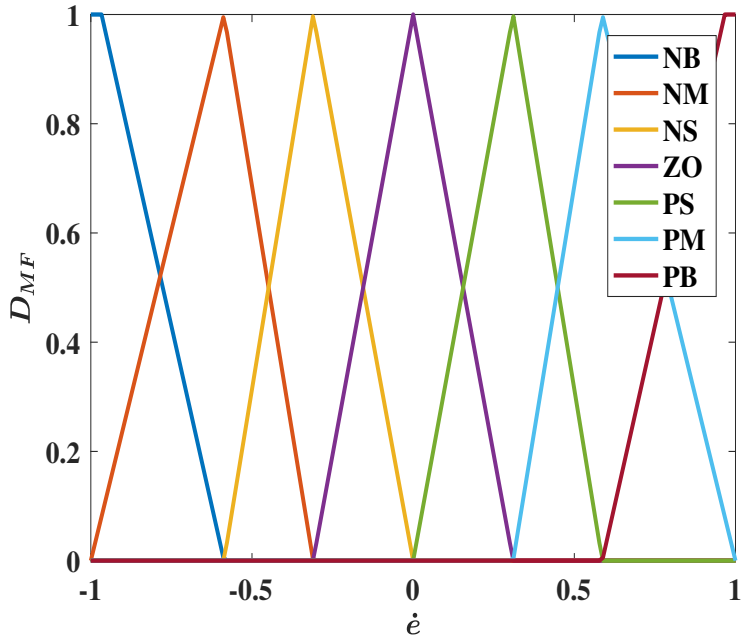

Figure 4.21 : Membership function distribution of derivative error.

These results have been achieved based on the GAO-TS optimization process. It can be seen that the domain of the membership functions which were demonstrated in Figure 3.9 to Figure 3.13 have been modified under the effect of this optimization process. The comparison of Figure 4.20 with Figure 3.12 shows the significant modification for the derivative of error input.

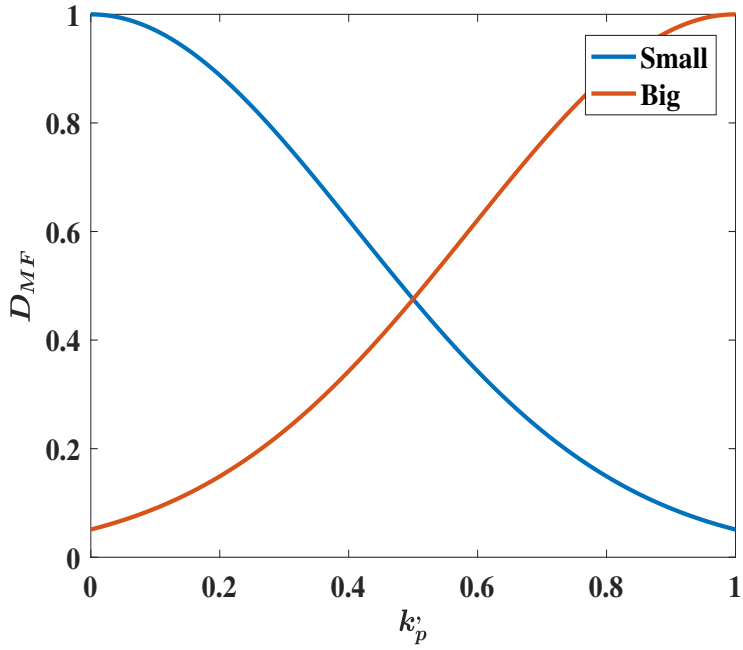

Figure 4.22 : Membership function distribution of $K_p{}'$.

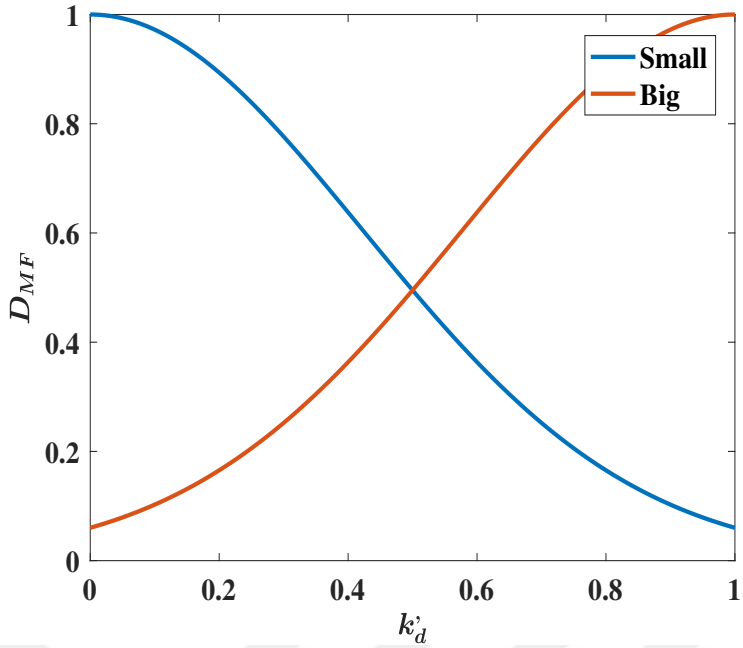

Figure 4.23 : Membership function distribution of $K_d{}'$.

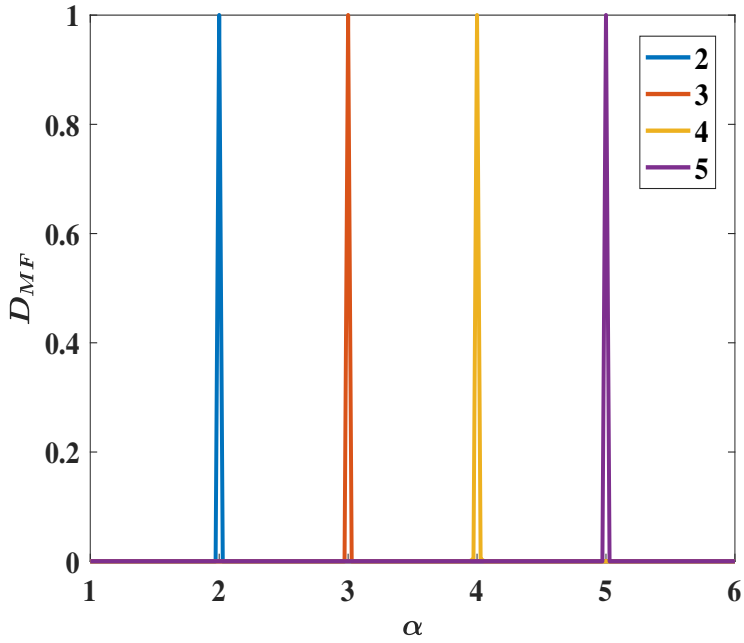

Figure 4.24 : Membership function distribution of α.

The comparison of the Figure 4.22 to Figure 4.24 with Figure 3.14 to Figure 3.16, respectively, shows the slight variation in the domain of the membership functions for the normalized proportional, derivative and integral gains. In order of having better understanding, Table 4.2 represents the domains of the membership functions for the inputs and outputs of the FIS and optimized FIS.

Table 4.2 : Comparison between the domains of the membership functions.

Variable	MF	FIS	Optimized FIS
e			
	NB	[-Inf -Inf -0.9667 -0.6667]	[-Inf -Inf -0.9667 -0.3326]
	NM	[-1 -0.6667 -0.3333]	[-1 -0.3326 -0.2825]
	NS	[-0.6667 -0.3333 0]	[-0.3326 -0.2825 0]
	ZO	[-0.3333 0 0.3333]	[-0.2825 0 0.2825]
	PS	[0 0.3333 0.6667]	[0 0.2825 0.3326]
	PM	[0.3333 0.6667 1]	[0.2825 0.3326 1]
	PB	[0.6667 0.9667 Inf Inf]	[0.3326 0.9667 Inf Inf]
$\dot{e}$			
	NB	[-Inf -Inf -0.9667 -0.6667]	[-Inf -Inf -0.9667 -0.5868]
	NM	[-1 -0.6667 -0.3333]	[-1 -0.5868 -0.3102]
	NS	[-0.6667 -0.3333 0]	[-0.5868 -0.3102 0]
	ZO	[-0.3333 0 0.3333]	[-0.3102 0 0.3102]
	PS	[0 0.3333 0.6667]	[0 0.3102 0.5868]
	PM	[0.3333 0.6667 1]	[0.3102 0.5868 1]
	PB	[0.6667 0.9667 Inf Inf]	[0.5868 0.9667 Inf Inf]
$K_d{}'$			
	Small	[0.4247 0]	[0.41 0]
	Big	[0.4247 1]	[0.41 1]
$K_d{}'$			
	Small	[0.4247 0]	[0.4217 0]
	Big	[0.4247 1]	[0.4217 1]
α			
	2	[1.95 2 2.05]	[1.976 2 2.024]
	3	[2.95 3 3.05]	[2.977 3 3.023]
	4	[3.95 4 4.05]	[3.972 4 4.028]
	5	[4.95 5 5.05]	[4.976 5 5.024]

After applying the optimized FIS into the fuzzy-PID controller, three considered PID's have been compared with each other for the same step response. Figure 4.25 depicts this comparison. It can be concluded from this figure and details listed in Table 4.3, the optimized fuzzy-PID controller has the significant OS reduction related to normal and fuzzy-PID controllers. In Table 4.3, the slight increase in the OS can be seen in the optimized fuzzy-PID controller with respect to the fuzzy-PID controller. However, since the normalization of the cost function including OS, RT and ST in the optimization procedure has been followed, therefore, the normalization of the cost function based on equation (3.24) and the values listed in the aforementioned table should be considered for comparison.

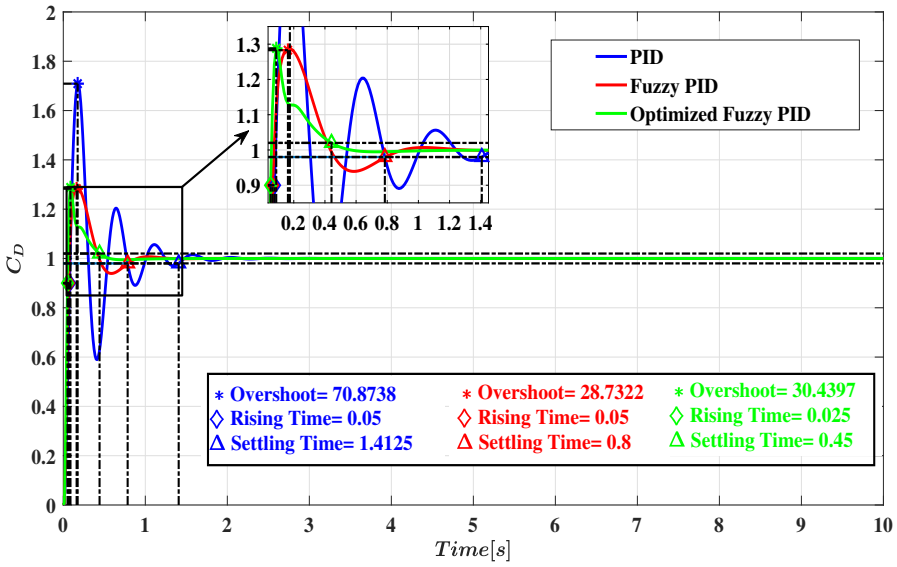

Figure 4.25 : Comparison of the step response of three considered PID controllers.

Table 4.3 : Comparison of characteristics of three considered PID controller.

PID types	OS	RT	ST
Normal	70.87382	0.05	1.4125
Fuzzy	28.7322	0.05	0.8
Optimized Fuzzy	30.4397	0.025	0.45

Based on following equations (4.1) and (4.2), it can be concluded that the normalized value of the cost function for the optimized fuzzy-PID controller is less than for the fuzzy-PID controller.

$$CF^{norm}_{OptFPID} = \frac{28.7322 - 25.2238}{25.2238} + \frac{0.8 - 0.35}{0.35} + \frac{0.05 - 0.125}{0.0125} = 4.4248 \qquad (4.1)$$

$$CF^{norm}_{FPID} = \frac{30.4379 - 25.2238}{25.2238} + \frac{0.45 - 0.35}{0.35} + \frac{0.025 - 0.125}{0.0125} = 1.492428 \qquad (4.2)$$

4.5 Coupling FLUENT and SIMULINK

The optimized fuzzy-PID controller was investigated where SIMULINK operation is defined to continue for 1.5 second. As can be seen in Figure 4.26, the desired value for the drag coefficient has been reached at the end of this considered time period.
Furthermore, it is evident from Figure 4.27 that the optimized fuzzy-PID controller has reached the considered drag coefficient in the BFS for Re=400 by changing the amplitude for the synthetic jet.

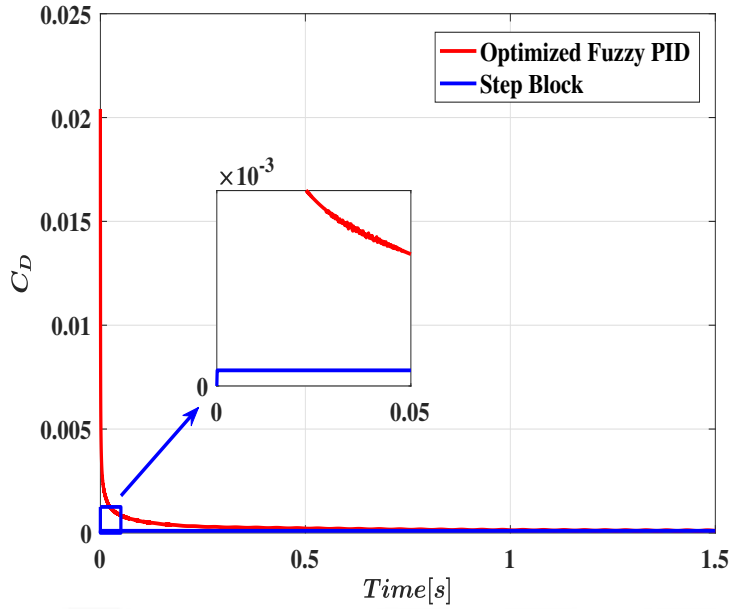

Figure 4.26 : Step response of the Optimized fuzzy-PID controller for Re=400.

Figure 4.27, additionally, represents that applying the optimized fuzzy-PID controller leads to nearly eliminate the fluctuation of the drag coefficient and consequently excessive required energy demand. Therefore. this leads to increase the efficiency of the system. However, for the system without considering optimized fuzzy-PID controller, the fluctuation of drag coefficient can be seen.

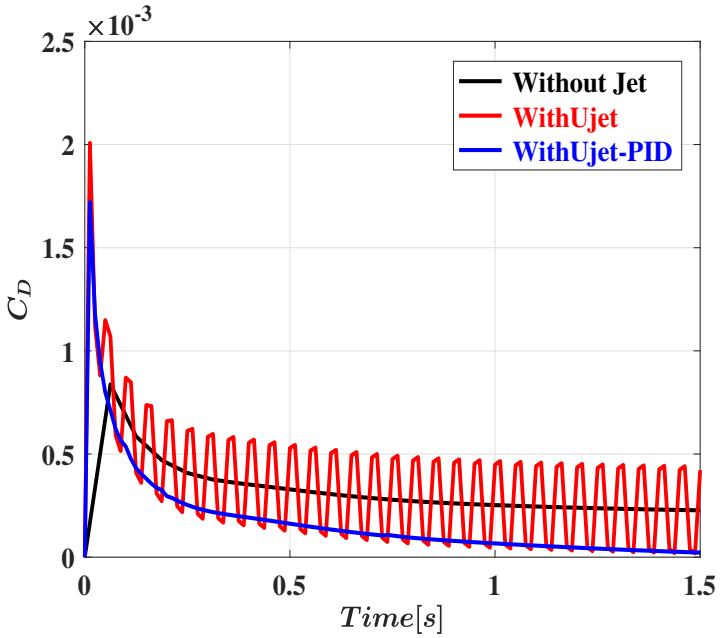

Figure 4.27 : Comparison of the average drag coefficient variation with respect to considered time period for Re=400.

The comparison of the skin friction coefficient with respect to the relative distance from the step has been carried out between the gathered results. This comparison is shown in Figure 4.28. It can be seen that the case with optimized fuzzy-PID controller has less value of the recirculation length in comparison with other cases. Additionally, even though the recirculation length for [2 -1 -1] and [0 -2 2] cases were smaller with respect to the optimized fuzzy-PID controller model, these cases have the lack of stability in drag coefficient which causes demand for more energy leading to less efficiency. The values of the recirculation for the conducted cases of studies have been demonstrated in Table 4.4.

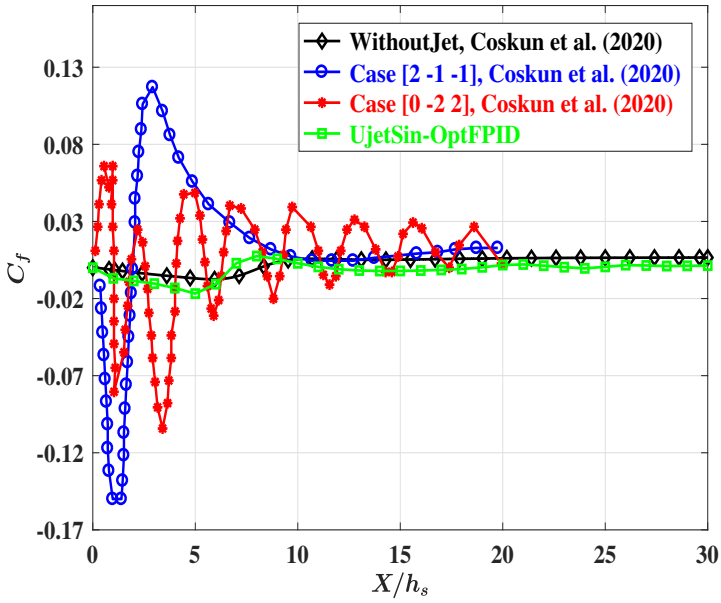

Figure 4.28 : Comparison of the skin friction coefficient of the conducted configurations.

Table 4.4 : Comparison of the recirculation length.

Configuration	Recirculation Length $[X/h_s]$
Without jet	8.1725
With jet (Optimized fuzzy-PID)	6.7507

From aforementioned table, it can be concluded that the flow separation and consequently recirculation length have been decreased 17.35% for the with-jet case with optimized fuzzy-PID controller (with-jet-OptFPID) with respect to the without-jet case of study.

4.6 Flow Field Simulations

Since three cases of studies have been conducted in different configurations, the comparison between these cases is mandatory to understand the improvement through the process. Figure 4.29 to Figure 4.31 demonstrate the velocity in the streamwise direction for without-jet, with-sinusoidal jet and with-jet-OptFPID cases of studies at Re=400.

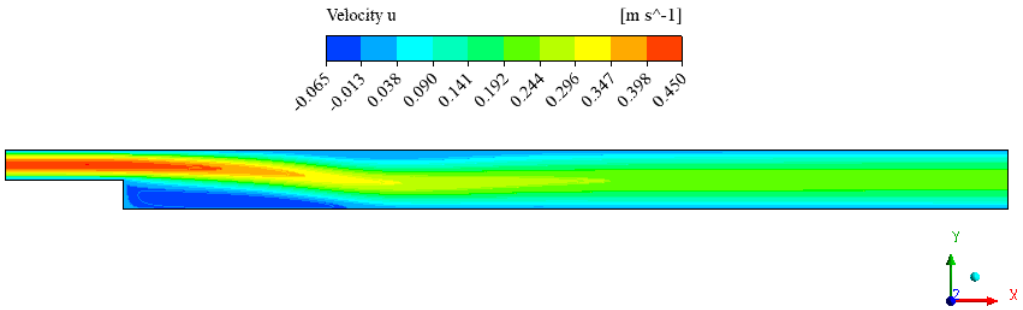

Figure 4.29 : Streanwise velocity in without jet case of study at Re=400.

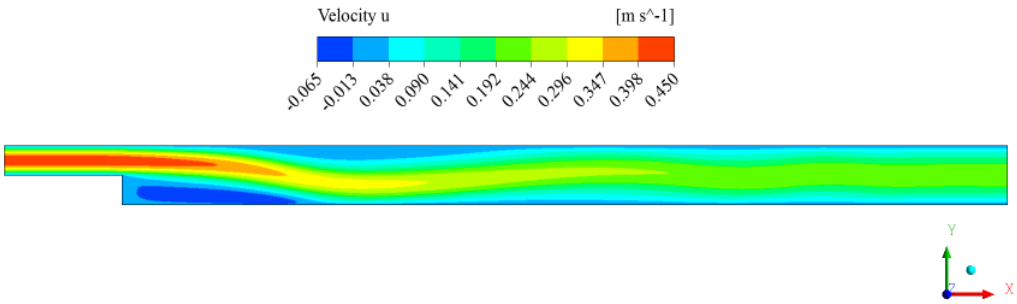

Figure 4.30 : Streanwise velocity in with sinusoidal jet case of study at Re=400.

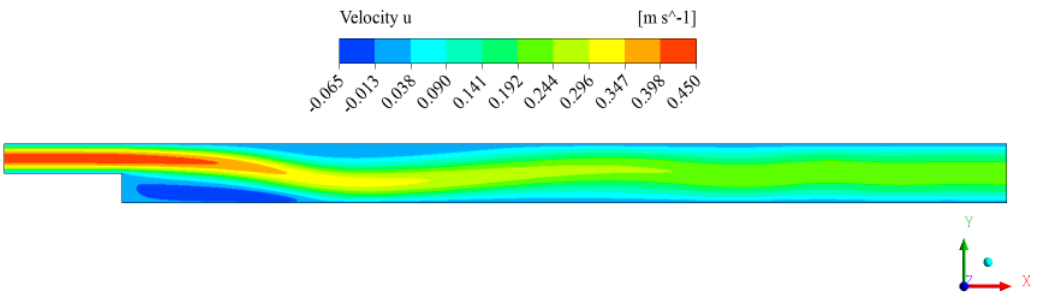

Figure 4.31 : Streanwise velocity in with sinusoidal jet case of study with applied optimized fuzzy-PID controller at Re=400.

The variation of the jet velocity versus time during the simulation when the optimized fuzzy-PID controller has been applied is shown in the Figure 4.32. It can be seen that during the flow time, the domain of the jet velocity has been changed in order of reaching the considered drag coefficient which has been considered. The comparison between Figure 4.27 and Figure 4.32 shows that this increasing pattern of the jet velocity has been effective in reducing the drag coefficient than the normal constant fluctuating sinusoidal pattern. Furthermore, the monotonously changing of the amplitude leads to eliminating the fluctuating of the drag coefficient and excessive energy. This conclusion can be clarified by the comparison of the jet velocity shown in Figure 4.33 for the with and without optimized fuzzy-PID controller.

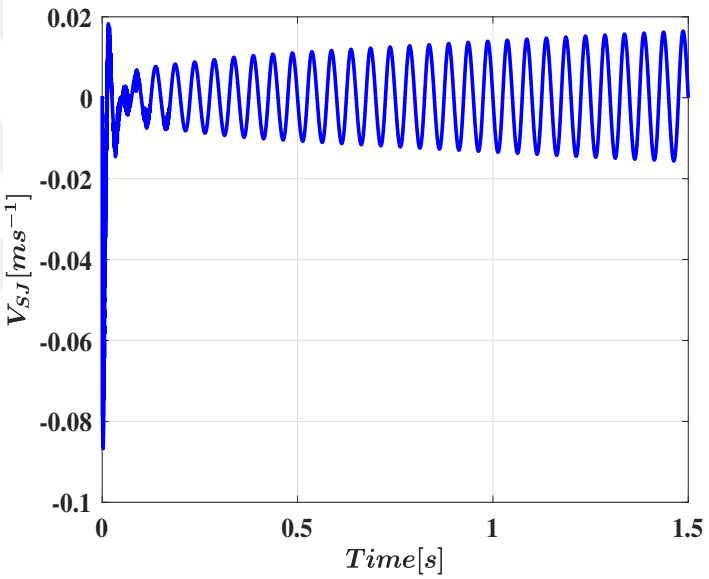

Figure 4.32 : Variation of the jet velocity versus time in the case with optimized fuzzy-PID controller at Re=400.

The comparison of vortices between the without-jet and with-jet-OptFPID cases of studies has been conducted in the following where the dimension of the secondary vortex is discussed as the criterion. For the with-jet-OptFPID case of study, the last cycle in the sinusoidal pattern including five time steps have been chosen for investigation. These time steps have been named $\delta t-4$, $\delta t-3$, $\delta t-2$, $\delta t-1$ and δt consecutively and they represent the neutralized (meaning neither suction nor blowing), suction, neutralized, blowing and neutralized states respectively. This identification has been clarified in Figure 4.34. The streamlines of the flow, along with

primary and secondary recirculation areas (vortices) have been illustrated in Figure 4.35 for the without-jet case of study.

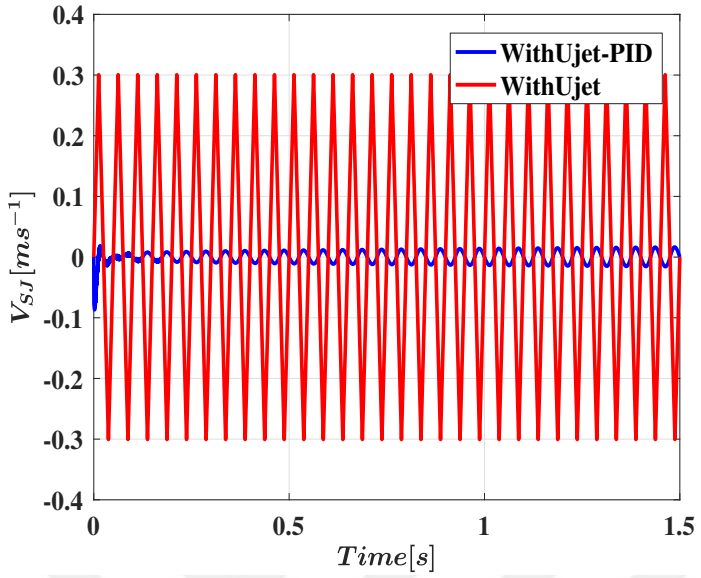

Figure 4.33 : Comparison of the jet velocity versus time in the case with and without optimized fuzzy-PID controller at Re=400.

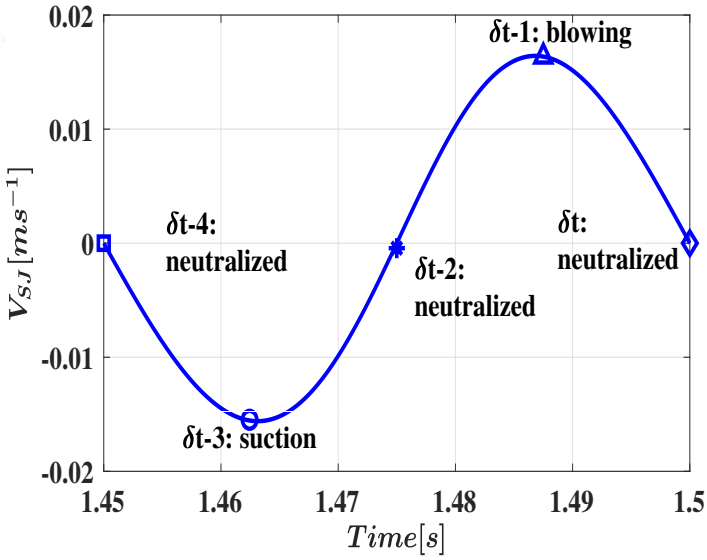

Figure 4.34 : Schematic of physical status of the synthetic jet at the last time step.

Generally, the shear layer which had been created after the step in the without-jet case of study disturbed by introducing the jet. The momentum injection interacts with the shear layer vortices leads to the reduction of the primary vortex and consequently shortening of the reattachment length.

Additionally, forcing amplitude near the separation edge enhances the shear layer growth in the perpendicular direction of the main flow and creates a large roll-up vortex. This causes the growth of the boundary layer thickness toward the step wall while reducing the reattachment length as well [41]. This phenomenon coupling with the monotonously sinusoidal increasing of the amplitude in the with-jet-OptFPID case of study, has become more effective in thickening the boundary layer and reducing the recirculation length. Therefore, more reduction of recirculation length and drag coefficient in this strategy has been occured. Variation of the streamlines in addition to vortices have been demonstrated for the last cycle of the with-jet-OptFPID from Figure 4.36 to Figure 4.40. Additionally, the dimensional comparison of the vortex created on the top wall of the computational domain is carried out. For the without-jet case of study, the height and width of the secondary (corner) vortex is constant in the considered time period and is about $0.11h_s$.

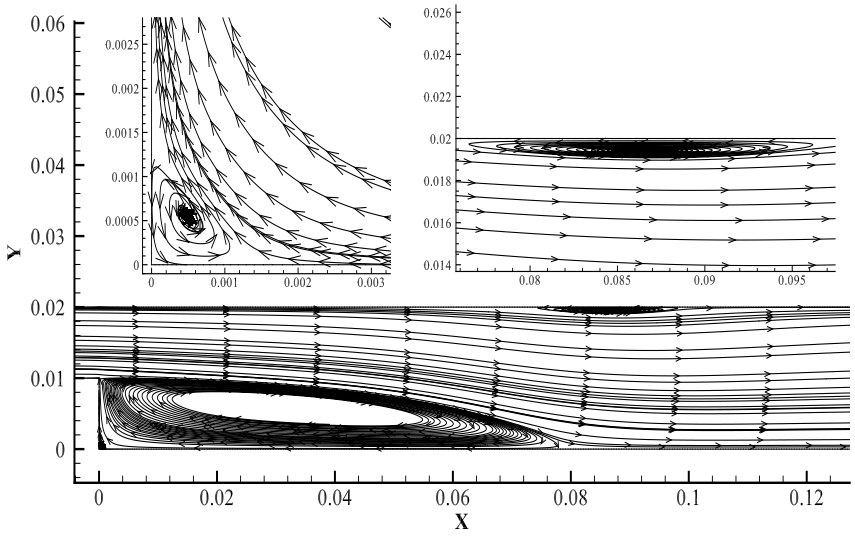

Figure 4.35 : Stream lines of flow in the without-jet case for Re=400.

However, for the with-jet-OptFPID case of study, the secondary vortex has different height and width values in each time step. In Figure 4.36 related to $\delta t - 4$ which is in the neutralized state, there was no corner vortex. Figure 4.37 represents the $\delta t - 3$ time step which is the suction state of the synthetic jet. The height and the width of the corner vortex in this figure becomes $0.03h_s$ and $0.04h_s$ respectively. Figure 4.38 illustrates the next consecutive time step, $\delta t - 2$, which is a neutralized state of the

synthetic jet. The secondary vortex in this figure has grown where the width and the height of the vortex are both about $0.25h_s$.

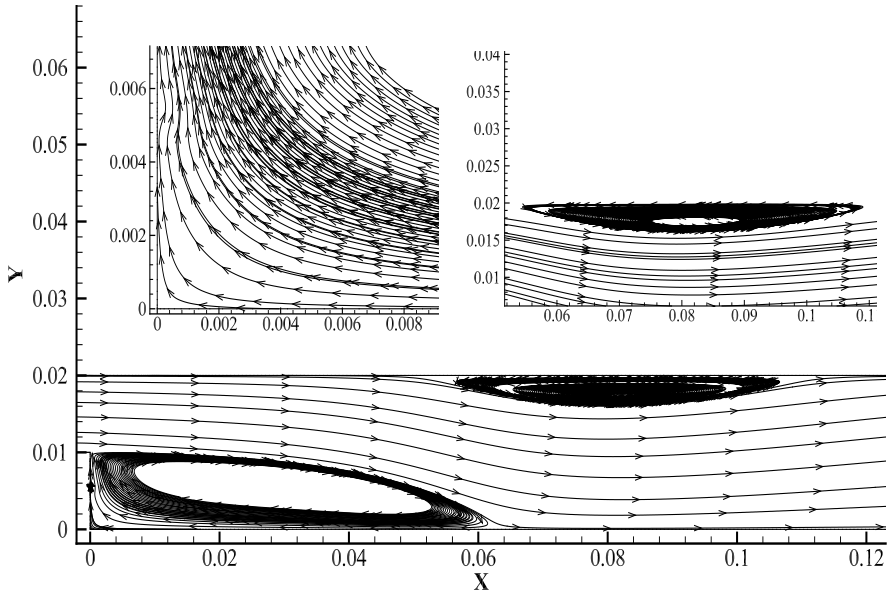

Figure 4.36 : Stream lines of flow in the with-jet-OptFPID case at $\delta t - 4$ for Re=400.

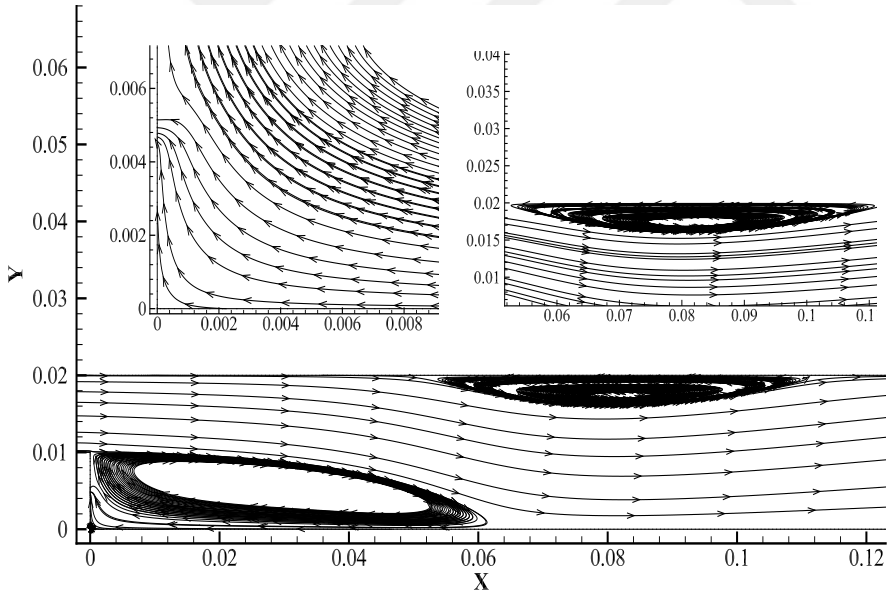

Figure 4.37 : Stream lines of flow in the with-jet-OptFPID case at $\delta t - 3$ for Re=400.

It should be pointed out that in this time step, the third vortex below the velocity inlet domain of the synthetic jet has been created due to switching from the suction to blowing state. The width and height of this vortex are about $0.03h_s$ and $0.07h_s$. Figure 4.39 depicts the $\delta t - 1$ time step which is the blowing state. The width and height of the secondary vortex in this time step have expanded to about $0.3h_s$.

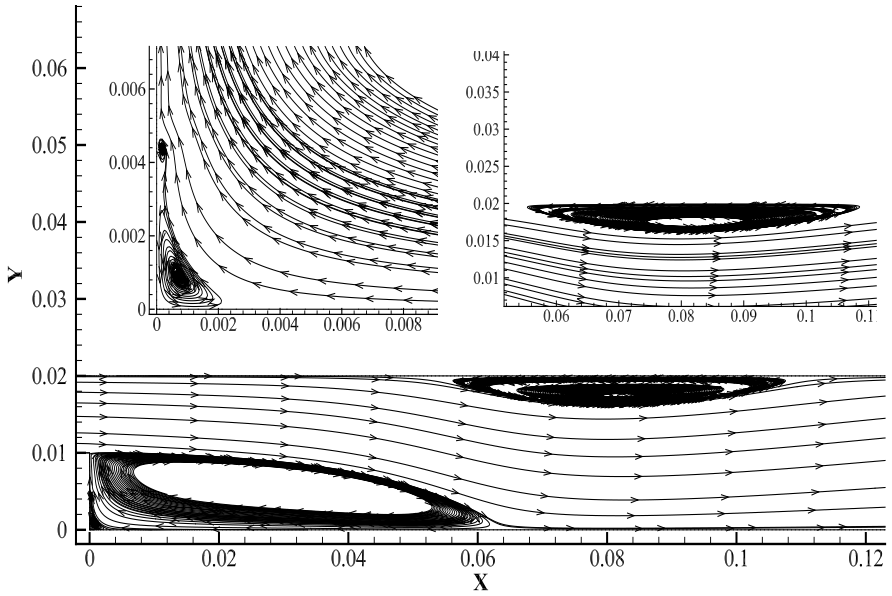

Figure 4.38 : Stream lines of flow in the with-jet-OptFPID case at $\delta t - 2$ for Re=400.

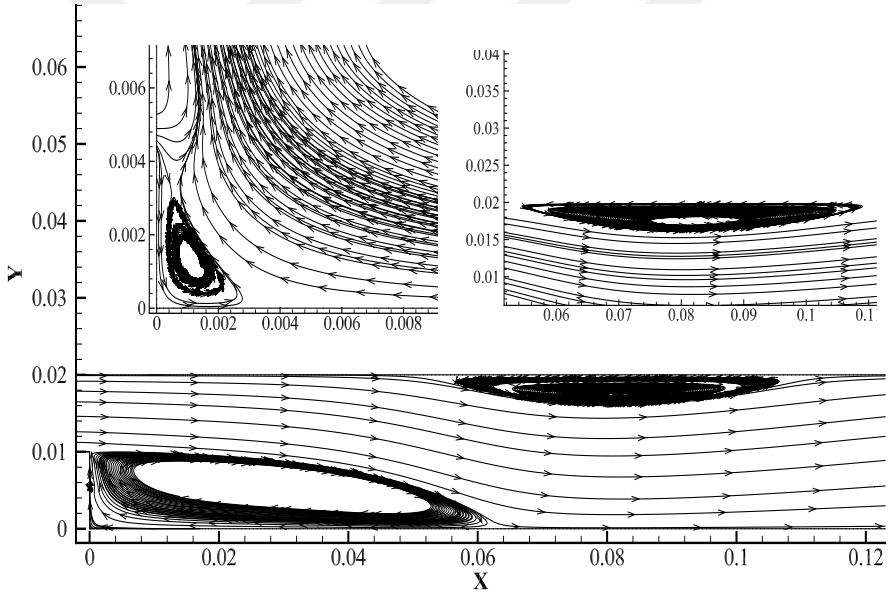

Figure 4.39 : Stream lines of flow in the with-jet-OptFPID case at $\delta t - 1$ for Re=400.

In the final considered time step (δt), which has been shown in Figure 4.40, synthetic jet is in the neutralized state where the secondary vortex has been eliminated. Worth to be noticed that the same flow pattern has been repeated in Figure 4.36 for the $\delta t - 4$ time step. Based on previous investigated cycles, it can be stated that in the neutralized state when blowing switches to suction, the secondary vortex become contracted and eventually eliminated. However, in the neutralized state where suction switches to blowing, the secondary vortex has expanded both in width and height.

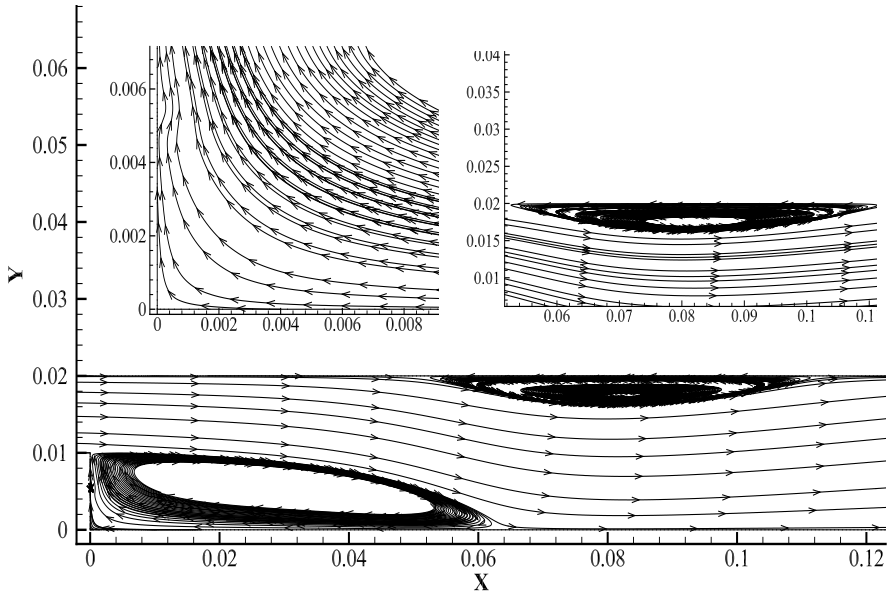

Figure 4.40 : Stream lines of flow in the with-jet-OPtFPID case at δt for Re=400.

For one complete cycle of the sinusoidal function of the synthetic jet, the same procedure has been followed in the previous time steps as well. It can be concluded that with-jet-OptFPID case of study has the higher value of width and height for the secondary (corner) vortex with respect to the without-jet case of study. The higher value of heights and width of the secondary vortex is the demonstration of the moving recirculation region toward the step wall and reducing the recirculation length. As mentioned earlier, there is a vortex at the top wall of the BFS as well. Based on Figure 4.35, the height and width of this vortex for the without-jet case of study is about $0.1h_s$ and $2.4h_s$ respectively while based on Figure 4.36 to Figure 4.40, the average width and height of this reciculation region for the with-jet-OptFPID case of study is about $0.4h_s$ and $6h_s$ respectively.

5. CONCLUSSION AND RECOMMENDATION

5.1 Conclusion

The BFS has been considered as the benchmark problem to investigate the modified PID controller in reducing the flow separation and drag coefficient. The numerical analysis is conducted for the validation of the with-jet and without-cases of studies. The accuracy which is achieved for both cases of validation was about 10%. The FIS is designed based on considering error and derivative of error as the inputs and gains of the PID controller as outputs. It has been concluded that the designed FIS is a desirable alternative in tuning the gains of the PID controller instead of conventional Z-N tuning method. The magnitudes of the OS and ST have been reduced 59.46% and 43.36% respectively for the fuzzy-PID controller with respect to the Z-N tuning method. Optimized fuzzy-PID controller has been defined based on optimizing the index numbers of the applied rules, domain of the inputs, domain of the outputs and values of the stabilizing coefficients of the designed FIS. Therefore, two optimization methods of GAO and PSO for reducing the defined cost function in the fuzzy-PID controller have been applied. In GAO method, three different methods of selecting parents including RS, RWS and TS have been applied. Additionally, two methods of defuzzification including bisector and centroid were considered. The GAO method based on TS and bisector deffuzification reached the least value of 1.4925 for the normalized cost function and 44 for NFE in comparison with other configurations. Therefore, the obtained FIS from this optimization method is applied in the SIMULINK analysis. The comparison between three PID controllers including conventional, fuzzy and optimized fuzzy showed that the performance of the optimized fuzzy-PID controller is significantly higher than two others by having the least value of 0.025 *s* for the RT and 0.45 *s* for the ST. Rising and settling times have been reduced 50 % and 43.75 % with respect to the fuzzy PID controller. The overshoot characteristic showed a slight increase. However, the value of normalized cost function for the

optimized fuzzy-PID controller was less than the fuzzy-PID controller. Afterwards, the SIMULINK coupled with ANSYS FLUENT CFD software based on applying the optimized fuzzy-PID controller was conducted. The results revealed that the size of the recirculation length of the BFS had been decreased 17.39 % in comparison with the without jet case of study. Additionally, reaching the settled value of the drag coefficient in the step point block of the SIMULINK model after defined time steps, explains the effectiveness of the optimized fuzzy-PID controller. Based on the defined value in step point block for the designed system, the optimized-fuzzy PID controller was able to control the velocity of the synthetic jet in a sinusoidal monotonously increasing manner that the drag coefficient reduced significantly as well with respect to other cases of study. Moreover, the fluctuations of drag coefficient demonstrated the unnecessary consuming energy for the case with sinusoidal jet without-PID case of study. This obstacle has been eliminated in the applied method where the fluctuation of the drag coefficient has been reduced significantly. The vortex analysis proves that the corner vortex created in the with-jet-OptFIP case of study has the higher width and height with respect to the without-jet case of study. This implies the growth of the recirculation region toward the step wall and consequently decreasing the recirculation length.

5.2 Recommendations

1. The study could be expanded to turbulent flow region to have a better view over the applicability of the proposed method for controlling the synthetic jet utilizing the optimized fuzzy-PID controller.
2. The study could be conducted with applying multiple input-output fuzzy-PID controller where other outputs could be defined such as value of the heat flux over the bottom wall after the step or value of the applied temperature over the bottom wall after the step. However, for this case, conducting CFD simulation based on applying the various constant heat flux or various temperature over the bottom wall would be necessary.
3. Other new methods of optimization could be considered for investigations in order of reaching less value of cost function with less computing time.
4. Considering three sinusoidal jet in the locations which had been studied with Coskun et al. 2021 and applying the multiple optimization methods for reaching the optimum

value of frequency and amplitude for the jets.

5. Considering the heat flux as another variable and studying the variation of the Nusselt number based on considered optimization methods in this study.

REFERENCES

[1] **Subaşı, A.** (2017). Numerical and experimental investigation of boundary layer transition with active and passive flow control methods, *Ph.D. Dissertation*, Istanbul Technical University.

[2] **Spazzini, P.G.**, **Iuso, G.**, **Onorato, M.**, **Zurlo, N. and Di Cicca, G.** (2001). Unsteady behavior of back-facing step flow, *Experiments in Fluids*, *30*(5).

[3] **Chen, L.**, **Asai, K.**, **Nonomura, T.**, **Xi, G. and Liu, T.** (2018). A review of backward-facing step (BFS) flow mechanisms, heat transfer and control, *Thermal Science and Engineering Progress*, *6*(5).

[4] **Iwai, H.**, **Nakabe, K. and Suzuki, K.** (2000). Flow and heat transfer characteristics of backward-facing step laminar flow in a rectangular duct, *International Journal of Heat and Mass Transfer*, *43*(3).

[5] **Saambavi, K.**, (2014). Flow Separation Control Using Synthetic Jets on a Flat Plate, M.Sc. Thesis, Embry–Riddle Aeronautical University.

[6] **Al-Jelawy, H.**, **Kaczmarczyk, S.**, **AlKhafaji, D.**, **Mirhadizadeh, S.**, **Lewis, R. and Cross, M.** (2016). A computational investigation of a turbulent flow over a backward facing step with OpenFOAM, *9th International Conference on Developments in eSystems Engineering (DeSE)*, Liverpool, England.

[7] **Dejoan, A. and Leschziner, M.** (2004). Large eddy simulation of periodically perturbed separated flow over a backward-facing step, *International Journal of Heat and Fluid Flow*, *25*(4).

[8] **Gautier, N.**, (2014). Flow control using optical sensors, M.Sc. Thesis, Université Pierre et Marie Curie-Paris VI.

[9] **Vea, A.**, (2012). Modelling of Adaptive Geometry Flow Control Solutions in CFD, M.Sc. Thesis, Institutt for energi-og prosessteknikk.

[10] **Cattafesta, L.N. and Sheplak, M.** (2011). Actuators for active flow control, *Annual Review of Fluid Mechanics*, *43*(1).

[11] **Fiedler, H. and Fernholz, H.H.** (1990). On management and control of turbulent shear flows, *Progress in Aerospace Sciences*, *27*(4).

[12] **Glezer, A. and Amitay, M.** (2002). Synthetic jets, *Annual review of fluid mechanics*, *43*(1).

[13] **Okada, K.**, **Fujii, K.**, **Miyaji, K.**, **Oyama, A.**, **Nonomura, T. and Asada, K.** (2010). Computational study of the synthetic jet on separated flow over a backward-facing step, *ASME International Mechanical Engineering Congress and Exposition*, Vancouver, British Columbia, Canada.

[14] **Tang, H. and Zhong, S.** (2006). Incompressible flow model of synthetic jet actuators, *AIAA journal*, *43*(4).

[15] **Xu, F.**, **Gao, Z.**, **Ming, X.**, **Xia, L.**, **Wang, Y.**, **Sun, W. and Ma, R.** (2015). The optimization for the backward-facing step flow control with synthetic jet based on experiment, *Experimental Thermal and Fluid Science*, *64*(4).

[16] **Ziegler, J.G. and Nichols, N.B.** (1993). Optimum Settings for Automatic Controllers, *Journal of Dynamic Systems, Measurement, and Control*, *115*(2B).

[17] **Pathmanathan, E. and Ibrahim, R.** (2010). Development and implementation of fuzzy logic controller for flow control application, *2010 International Conference on Intelligent and Advanced Systems*, Kuala Lumpur, Malaysia.

[18] **Zhao, Z.Y.**, **Tomizuka, M. and Isaka, S.** (1993). Fuzzy gain scheduling of PID controllers, *IEEE transactions on systems, man, and cybernetics*, *23*(5).

[19] **Jahedi, G. and Ardehali, M.** (2011). Genetic algorithm-based fuzzy-PID control methodologies for enhancement of energy efficiency of a dynamic energy system, *Energy Conversion and Management*, *52*(1).

[20] **Kennedy, J. and Eberhart, R.** (1995). Particle swarm optimization, *Proceedings of ICNN'95-international conference on neural networks*, Perth, WA, Australia.

[21] **Roos, F.W. and Kegelman, J.T.** (1986). Control of coherent structures in reattaching laminar and turbulent shear layers, *AIAA journal*, *24*(12).

[22] **Bhattacharjee, S.**, **Scheelke, B. and Troutt, T.** (1986). Modification of vortex interactions in a reattaching separated flow, *AIAA journal*, *24*(4).

[23] **Louda, P.**, **Příhoda, J.**, **Kozel, K. and Sváček, P.** (2013). Numerical simulation of flows over 2D and 3D backward-facing inclined steps, *International journal of heat and fluid flow*, *43*(4).

[24] **Ötügen, M.** (1991). Expansion ratio effects on the separated shear layer and reattachment downstream of a backward-facing step, *Experiments in fluids*, *10*(5).

[25] **Gautier, N. and Aider, J.L.** (2013). Control of the separated flow downstream of a backward-facing step using visual feedback, *Proceedings of the Royal Society A: Mathematical, Physical and Engineering Sciences*, *469*(2160), https://doi.org/10.1098/rspa.2013.0404.

[26] **Armaly, B.F.**, **Durst, F.**, **Pereira, J. and Schönung, B.** (1983). Experimental and theoretical investigation of backward-facing step flow, *Journal of fluid Mechanics*, *127*(5).

[27] **Coskun, U.**, **Cadirci, S. and Gunes, H.** (2021). Numerical Investigation of Active Flow Control on Laminar Forced Convection over a Backward Facing Step Surrounded by Multiple Jets, *Journal of Applied Fluid Mechanics*, *14*(2).

[28] **Uruba, V.**, **Jonáš, P. and Mazur, O.** (2007). Control of a channel-flow behind a backward-facing step by suction/blowing, *International Journal of Heat and Fluid Flow*, *14*(4).

[29] **Chun, K.B. and Sung, H.J.** (1996). Control of turbulent separated flow over a backward-facing step by local forcing, *Experiments in fluids*, *21*(6).

[30] **Guo, G.m.**, **Liu, H. and Zhang, B.** Numerical study of active flow control over a hypersonic backward-facing step using supersonic jet in near space.

[31] **Timoshenko, S.**, **Woinowsky-Krieger, S.** *et al.* (1959). *Theory of plates and shells*, McGraw-hill New York, USA.

[32] **Tayyaba, S.**, **Afzal, M.J.**, **Sarwar, G.**, **Ashraf, M.W. and Afzulpurkar, N.** (2016). Simulation of flow control in straight microchannels using fuzzy logic, *2016 International Conference on Computing, Electronic and Electrical Engineering (ICE Cube)*, Quetta, Pakistan.

[33] **Bassi, S.**, **Mishra, M. and Omizegba, E.** (2011). Automatic tuning of proportional-integral-derivative (PID) controller using particle swarm optimization (PSO) algorithm, *International Journal of Artificial Intelligence & Applications*, *2*(4).

[34] **Mantri, G. and Kulkarni, N.** Design and optimization of PID controller using genetic algorithm.

[35] **Mirzal, A.**, **Yoshii, S. and Furukawa, M.** PID parameters optimization by using genetic algorithm.

[36] **Chiou, J.S.**, **Tsai, S.H. and Liu, M.T.** (2012). A PSO-based adaptive fuzzy PID-controllers, *Simulation Modelling Practice and Theory*, *26*(6).

[37] **Solihin, M.I.**, **Tack, L.F. and Kean, M.L.** (2011). Tuning of PID controller using particle swarm optimization (PSO), *Proceeding of the international conference on advanced science, engineering and information technology*, Hotel Equatorial Bangi-Putrajaya, Malaysia.

[38] **Jain, H.**, **Agarwal, R. and Cary, A.** (2003). Numerical Simulation of the Influence of a Synthetic Jet on Recirculating Flow Over a Backward Facing Step, *41st Aerospace Sciences Meeting and Exhibit*, Reno, Nevada.

[39] **Yousefi, T.**, **Karami, A.**, **Rezaei, E. and Ebrahimi, S.** (2012). Fuzzy modeling of the forced convection heat transfer from a V-shaped plate exposed to an air slot jet, *Heat Transfer—Asian Research*, *41*(5).

[40] **Marler, R.T. and Arora, J.S.** (2004). Survey of multi-objective optimization methods for engineering, *Structural and multidisciplinary optimization*, *26*(6).

[41] **Sujar-Garrido, P.**, **Benard, N.**, **Moreau, E. and Bonnet, J.** (2015). Dielectric barrier discharge plasma actuator to control turbulent flow downstream of a backward-facing step, *Experiments in Fluids*, *56*(4).

CURRICULUM VITAE

Name Surname : HAMED RAHMATI AYDENLOU

EDUCATION :

- **B.Sc.** : 2012, Urmia University, Faculty of Agricultural Engineering, Department of Mechanical Engineering of Biosystem
- **M.Sc.** : 2015, Urmia University, Faculty of Agricultural Engineering, Department of Mechanical Engineering of Biosystem

PROFESSIONAL EXPERIENCE AND REWARDS:

- 2010-2012, Urmia University, BioEnergy Lab.
- 2011 Teacher Assistant, Fluid Mechanics, Urmia University
- 2012 Teacher Assistant, Strength of Material, Urmia University
- 2021-2022 Research Assistant, RWTH Aachen University

PUBLICATIONS, PRESENTATIONS AND PATENTS ON THE THESIS:

- **Rahmati Aidinlou, H., and Nikbakht, A. M.** 2017. Design, Construction and Evaluation of Solar Flat-Plate Collector Simulator Based on the Thermohydraulic Coefficient., *JOURNAL OF AGRICULTURAL MACHINERY*.

- **Rahmati Aidinlou, H., and Nikbakht, A. M.** 2017. Heat Flux: Thermohydraulic Investigation of Solar Air Heaters Used in Agro-Industrial Applications., *Heat and Mass Transfer/Waerme- und Stoffuebertragung* 53(3), 917—928.

- **Rahmati Aidinlou, H., and Nikbakht, A. M.** 2019. Intelligent Modeling of Thermohydraulic Behavior in Solar Air Heaters with Artificial Neural Networks., *Neural Computing and Applications* 31(8), 3279–3293.

- **Rahmati Aidinlou, H., and Nikbakht, A. M.** 2022. Fuzzy-based modeling of thermohydraulic aspect of solar air heater roughened with inclined broken roughness., *Neural Computing and Applications* 34(3), 2393–2412.

HAMED RAHMATI AYDENLOU	CLOSED-LOOP FLOW SEPARATION CONTROL IN THE BACKWARD FACING STEP FLOW USING FUZZY-BASED PID CONTROLLER	2022